THE LIGAND DEPENDENT LUMINESCENT PROPERTIES OF A LANTHANIDE-BASED COMPLEX TO STUDY AND OPTIMIZE ITS USE AS A BIOMEDICAL LABEL.

A thesis presented to the faculty of the Graduate School of Western Carolina University in partial fulfillment of the requirements for the degree of Master of Science in Chemistry.

By

Sarah Marie Ryder

Director: Dr. Brian Dinkelmeyer
Associate Professor of Chemistry
Department of Chemistry and Physics

Committee Members: Dr. Channa De Silva, Dr. Al Fischer

July 2021

ACKNOWLEDGEMENTS

I would like to express my gratitude and acknowledgments to my committee chair, Dr. Brian Dinkelmeyer, and committee members, Dr. Channa De Silva and Dr. Al Fischer, for all their insight, advice, and for helping to answer my many questions. Thank you for pushing me to recognize and maximize my potential.

I would also like to offer my sincere appreciation for the learning opportunities provided by my committee and the rest of the faculty and staff within the Department of Chemistry and Physics at WCU. Without each one of these people and their efforts, this work wouldn't have been possible.

Lastly, I offer my warmest regards and thanks to all my family for their constant love and support, especially my parents and sister. The endless amount of encouragement from all my family and friends has motivated and inspired me throughout my work.

TABLE OF CONTENTS

LIST OF TABLES

LIST OF FIGURES

LIST OF ABBREVIATIONS

UV	Ultraviolet
UV-Vis	Ultraviolet-visible
NMR	Nuclear Magnetic Resonance
HNMR	Proton NMR
CNMR	Carbon NMR
IR	Infrared
FT-IR	Fourier-Transform Infrared
Ln^{3+}	Lanthanide (III)
DCM	Dichloromethane
DMSO	Dimethyl sulfoxide
TTA	Thenoyltrifluoroacetone
PIP	Phenyl-1H-imidazo[4,5-f][1,10]phenanthroline
2-tolu PIP	2-Tolu-1H-imidazo[4,5-f][1,10]phenanthroline
4-tolu PIP	4-Tolu-1H-imidazo[4,5-f][1,10]phenanthroline
2-CF_3 PIP	[2-triflouromethy-phenyl]-1H-imidazo[4,5-f][1,10]phenanthroline
4-CF_3 PIP	[4-triflouromethy-phenyl]-1H-imidazo[4,5-f][1,10]phenanthroline
2-nitro PIP	[2-nitro-phenyl]-1H-imidazo[4,5-f][1,10]phenanthroline
4-nitro PIP	[4-nitro-phenyl]-1H-imidazo[4,5-f][1,10]phenanthroline
2,4-disulfoxide PIP	4-(1H-imidazo[4,5-f]1,10-phenanthrolin-2-yl)benzene-1,3-disulfoxide **(2)**
4-amino PIP	4-(1H-imidazo[4,5-f]1,10-phenanthrolin-2-yl) p-aniline **(3)**
2-amino PIP	4-(1H-imidazo[4,5-f]1,10-phenanthrolin-2-yl) o-aniline **(4)**
4-hydroxy PIP	4-(1H-imidazo[4,5-f]1,10-phenanthrolin-2-yl) p-phenol **(5)**
2-hydroxy PIP	4-(1H-imidazo[4,5-f]1,10-phenanthrolin-2-yl) o-phenol **(6)**

ABSTRACT

THE LIGAND DEPENDENT LUMINESCENT PROPERTIES OF A LANTHANIDE-BASED COMPLEX TO STUDY AND OPTIMIZE ITS USE AS A BIOMEDICAL LABEL.

Sarah Marie Ryder, M.S.

Western Carolina University (July 2021)

Director: Dr. Brian Dinkelmeyer

The synthesis of novel electron donating and water-soluble ligands for Eu^{3+} coordination in efforts to optimize the luminescent properties of a europium TTA complex. Biomedical labeling with luminescent lanthanide complexes can be used to image and measure structural characteristics of proteins and other biological molecules with high spectral purity. This works aims to study structural variations of a PIP ligand that optimize the efficacy of a europium complex for its use as a fluorescent biomedical label. Each PIP ligand was synthesized from 1,10-Phenanthroline-5,6-dione and an aldehyde substituent to be further reacted with $Eu(TTA)_3.2H_2O$ to form the chelated europium complex. The structure of each PIP ligand was characterized using FT-IR, ^{1}H NMR, and ^{13}C NMR spectroscopy.

CHAPTER 1: INTRODUCTION

1.1. MOTIVATION

This work is in contribution to the therapeutic understanding of life science and aims to further study the ways in which structural and environmental characteristics of organometallic complexes can be applied to the development and design of biomedical agents.

1.2. BACKGROUND

1.2.1. Luminescent Lanthanide Labels

Luminescent lanthanide (Ln) complexes are being studied for their promising applications and potential advantages in biomedical labeling and imaging.[1] Ln metals in the form of free ions, such as europium (Eu^{3+}) and terbium (Tb^{3+}), have weak molar absorptivity due to LaPorte forbidden transitions of the f-orbital. Having an organic ligand strongly chelated to a Ln^{3+} metal sensitizes the Ln cation. The chelating ligand acts as the antenna to absorb incident light, prompting an energy transfer, and a luminescent emission results from the f-f electronic transitions of the Ln^{3+} center.[17, 7, 11] The fundamental structure of a luminescent lanthanide complex and the observable emission are both shown in Figure 1.

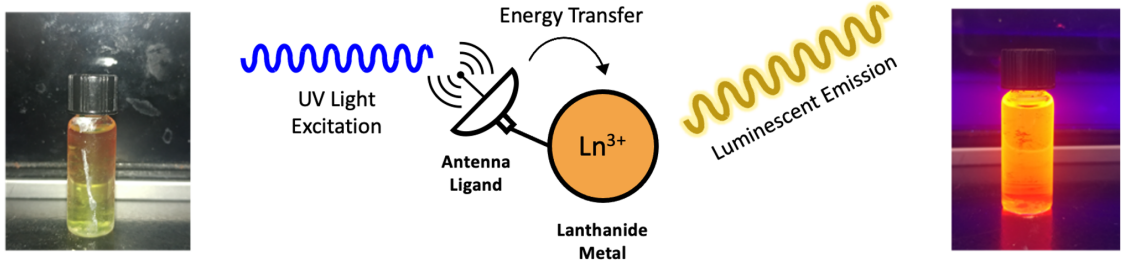

Figure 1. The antennae effect and visible emission of, $Eu(TTA)_3.2H_2O$, a chelated lanthanide complex before and after exposure to UV excitation.[1]

1.2.2. Spectroscopic Properties of Ln^{3+} Complexes

For Ln 3+ metals, most of the electron density resides in the 4f orbital, which is lower in energy, nested away from the surrounding environment and shielded by the further out electrons in the 5d and 6s orbitals. This shielding leads to diminished ligand field effects where the electrons in the 4f orbitals are not involved in bonding resulting in a fixed splitting between the f electronic levels.[17] Due to this fixed energy gap, the wavelength of light emitted by the complex does not change, regardless of the chelated ligand field. The fixed emission wavelength allows chelated ligands to be modified without affecting the emission wavelength of the complex, a highly advantageous tool for biomedical imaging and labeling techniques.

Using time resolved fluorescence spectroscopy, Ln^{3+} complexes can measure environmental interactions and conformational changes of proteins on a microsecond scale.[13] The antenna effect, large Stokes shifts, narrow emission bands, long luminescent lifetimes, and limited photobleaching are among the photo-physical properties that are unique to lanthanide complexes.[7] The optimized spectral purity of lanthanide complexes makes them of interest for their use as labels in bioassays.[18]

Narrow emission bands and large Stokes shift are characteristic to chelated Ln ions under the antenna effect. Both the absorption and emission spectra for a chelated europium complex, $Eu(TTA)_3.2H_2O$, are shown in Figure 2. The large gap between the wavelength of absorption and emission, referred to as the Stokes shift, allows little interference from incident light, and contributes to the spectral purity observed with chelated Ln^{3+} complexes.[7]

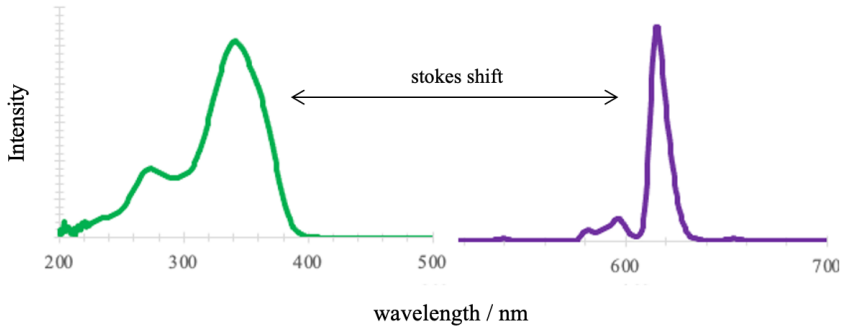

Figure 2. The absorbance and emission spectra for a lanthanide complex, $Eu(TTA)_3.2H_2O$, showing the large Stokes shift between the maximum light absorbance at 341 nm and the luminescent emission at 615 nm.

In biomedical imaging, traditionally used organic dyes have a detectable signal with a nanosecond lifetime after flash excitation. The detectable signal of organic dyes decays at a limiting rate when compared to the background noise, the interfering signals from intrinsically fluorescent proteins inside the body. Lanthanide labels have a relatively longer luminescent lifetime than traditionally used organic dyes. After flash excitation, lanthanide complexes have a detectable signal for approximately one millisecond before their emission starts to decay.[18] The signal from Ln^{3+} complexes can still be detected after all the background noise has decayed, around 25-30 microseconds. Time resolved fluorescence spectroscopy applies a delay period after flash excitation to allow the background noise to decay so that only the lanthanide luminescence is detected. This technique, illustrated in Figure 3, contributes to the spectral purity of biomedical imaging techniques by minimizing the amount of background noise that can interfere with the detected signal from the Ln^{3+} complex.[1, 23]

Photobleaching refers to the degradation of a fluorophore's optical properties over time and describes how the constant excitation to antibonding orbitals will eventually degrade and destroy the bonds. When a labeling complex absorbs light, electrons are excited to antibonding orbitals and relax back down to the ground state, some giving off a light. Due to photobleaching,

the observable period of detection for traditional fluorophores is significantly limited. Lanthanide probes, however, experience minimal photobleaching and can therefore be used repetitively for longer periods of time.[11]

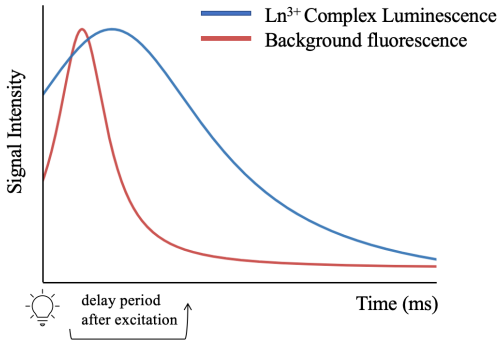

Figure 3. The concept of time resolved fluorescence spectroscopy, where the background fluorescence is resolved after 25-30 microseconds and the lanthanide labeling complex is still detected.[1]

For lanthanide complexes, the emission bands are narrow and line like.[17] In contrast, traditionally used organic dyes have broadband emissions.[23] This is observed when comparing a green emission from an organic fluorophore to the 544 nm emission from a lanthanide complex with Tb (III). Although both compounds emit green light, the narrow emission bands from the Ln^{3+} complex indicate a well-defined color of emission. The lanthanide metals in the 3+ oxidation state each emit a selectively narrow emission when molar absorptivity is achieved through the antenna effect.[17]. For example, complexes with the lanthanide Eu^{3+} have a 615 nm emission and Tb^{3+} have a 544 nm emission. This selectivity can be applied for multi-modal imaging materials so that the labeling of different chemical species can be observed in the same cell.[1]

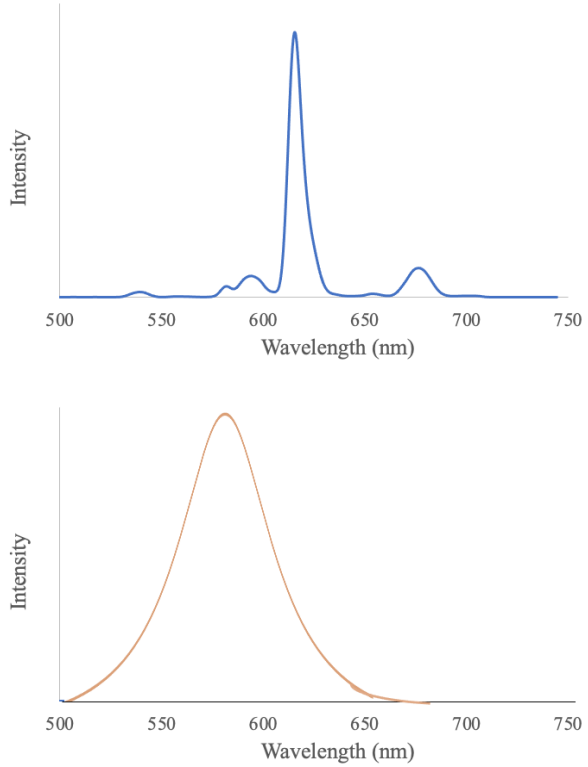

Figure 4. The broad emission spectrum observed with traditionally used fluorescent labels (bottom), compared to the narrow band in the top emission spectrum from a lanthanide complex with Eu (III).[23]

1.2.3. Electronic Transitions of Ln^{3+} Complexes

The diagram in Figure 5 shows the electronic pathway of energy transfer that takes place in the antenna effect, where an organic ligand acts as the antenna to absorb incident light and transfers electrical energy to the Ln center. Upon the absorption of light, as observed in Figure 5, an electron from the ligand ground state, S_0, is excited to a singlet state, S_1. Several relaxation processes are possible for the excited electron in S_1. The electron can relax back down to the ground state in the form of ligand fluorescence and other non-radioactive emissions, or the excited singlet state can undergo an intersystem crossing to occupy a slightly lower triplet state, T_1. The ligand-based triplet state can then relax back down to the ground state, S_0, in the form of

ligand phosphorescence and other non-radioactive emissions, or it can transfer energy to the Ln^{3+} centered $^5D_0$ excited state. The relaxation of the lanthanide excited state, $^5D_0$, to the ground state gives off a lanthanide centered emission.[1, 7]

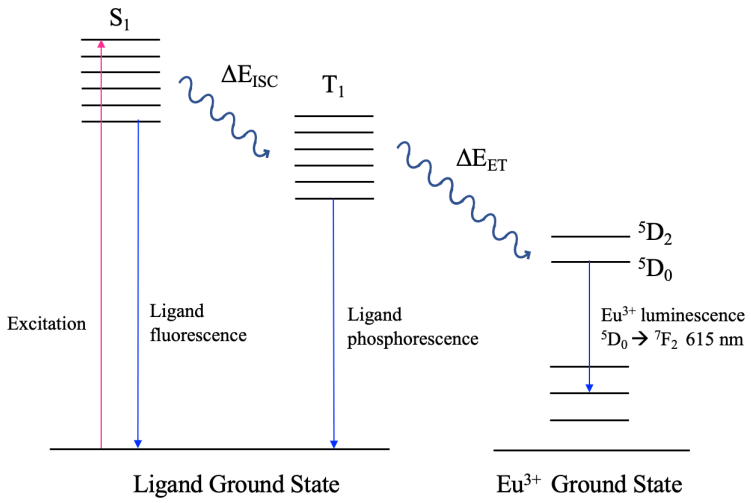

Figure 5. The electronic path of energy transfer associated with the antennae effect and luminescent emission from a europium chelated complex.[4]

Spectroscopic analysis of the absorption and emission of a Ln complex is used to measure the electronic transitions that result in luminescence. The first transition from the ground state to the excited singlet state, $S_0 \rightarrow S_1$, can be measured and the energies can be calculated from the absorption spectrum. The energy of intersystem crossing (ΔE_{ISC}) is the difference in energy between the ligand singlet state, S_1, and the slightly lower triplet state, T_1. The relaxation of the triplet state to the ground ligand state, $T_1 \rightarrow S_0$, results in the energy transfer (ΔE_{ET}) into the $^5D_1$ or $^5D_0$ excited state of the Ln^{3+} metal. The nature of the substituent (-R) on the ligand in complex will affect the ligand singlet state, S_1, and triplet state, T_1. This is dependent on whether the ligand is a sigma or a pi donor in its electronic behavior. Electron

donating functional groups are expected to raise the energies of ΔE_{ET} and ΔE_{ISC}, while electron withdrawing substituents are expected to lower the energies of the singlet state and triplet state. [7]

For electrons to transfer into the $^5D_0$ state, the lowest triplet state, T_1, must have an energy close to that of the $^5D_0$ state, 2.14493 eV.[7] The energy associated with the lowest triplet state is sensitive to the luminescent efficiency of Eu^{3+} complexes.[14] Recent studies using computational methods have additionally found that the associated energies of ΔE_{ET} and ΔE_{ISC} may correspond to the respective luminescent quantum yield of a lanthanide complex.[10]

The Ln^{3+} metal f-orbitals are highly shielded and are not involved in bonding, because of this the coordinated ligand only affects the energies of the ligand based S_1 and T_1 excited states, as well as the intensity of emission. The coordinated ligand will not affect the energy of the metal $^5D_0$ state or the wavelength of emission. This characteristic prompts the structural focus of this study, in that the complexed ligand structure can be modified to enhance and monitor the intensity of luminescence without altering the emission wavelength.[11, 17]

The fixed emission wavelength is a highly advantageous tool for biomedical imaging and labeling techniques. This allows for fine tuning of the ligand to optimize the emission intensity and binding properties of the Ln^{3+} complex. This works aims to synthesize structural variations of a chelating phenyl-1H-imidazo[4,5-f][1,10]phenanthroline (PIP) ligand to optimize the efficiency of a europium complex for its use as a fluorescent biomedical label. Specifically, novel electron donating, and water-soluble ligands have been synthesized and characterized for future Eu^{3+} coordination in efforts to optimize the luminescent properties of a europium TTA complex.

CHAPTER 2: EXPERIMENTAL

2.1. MATERIALS AND INSTRUMENTATION

Each PIP ligand was synthesized from 1,10-Phenanthroline-5,6-dione and a benzaldehyde substituent with structural variation, R. The PIP ligand was further reacted with $Eu(TTA)_3.2H_2O$ to form the chelated $Eu(TTA)_3PIP$ complex, as observed in Figure 6. The structure of each PIP ligand was characterized using FT-IR, H^1 NMR, and C^{13} NMR spectroscopy. All reagents were purchased from Sigma Aldrich, Fisher Science, Acros Organics, and used without further purification unless otherwise stated.

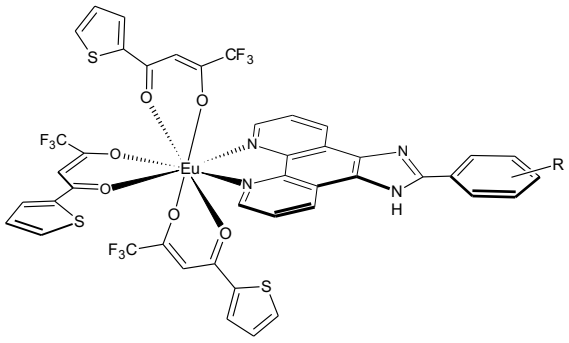

Figure 6. The $Eu(TTA)_3$ PIP complex with a Eu^{3+} metal chelated to both TTA and the sensitizing PIP ligand. The location of variation for the phenyl substitution is designated as R.

2.1.1. FT-IR Spectroscopy

FT-IR spectra were obtained for each of the PIP derived ligands to confirm the presence of various functional groups. Spectra were collected using a Perkin Elmer Spectrum One instrument equipped with a diamond attenuated total reflectance (ATR) cell. All measurements were performed at room temperature with a single bounce scanning range from 4000 cm^{-1} to 500

cm^{-1}. A background was acquired, prior to collecting each sample spectrum. All ligand samples were measured in their solid form. The ATR cell of the instrument was routinely cleaned with acetone and a Kimwipe before and between each measurement.

2.1.2. NMR Spectroscopy

^{1}H and ^{13}C NMR spectroscopy were performed using a JEOL 300 MHz Eclipse NMR with a 5 mm probe. For each of the PIP ligands, NMR samples were prepared by dissolving approximately 10 mg of solid product in deuterated dimethyl sulfoxide (d6-DMSO). ^{1}H NMR spectra were collected using 16 scans while ^{13}C NMR spectra were collected using 20,000 scans. ^{13}C NMR samples were prepared similarly, except material was added until the deuterated solution was saturated.

2.2. SYNTHESIS METHODS

*2.2.1. Synthesis of 1,10-phenanthroline-5,6-dione **(1)***

A mixture of 1,10-phenantroline (2.0116 g, 11.16 mmol, 1 equiv.) and potassium bromide (2.0886g, 17.45 mmol, 1.56 equiv.) was combined in a 100 ml round bottom flask and set up with a reflux condenser column. Concentrated sulfuric acid (20ml, 33.43equiv.) was slowly added to the reaction flask through the center of the condensing column, forming an orange gas. While stirring, fuming nitric acid (10ml, 21.46 equiv.) was added dropwise over a 15-minute period before the solution stirred overnight while under reflux. Upon cooling, the solution was poured over ice in a 500 ml beaker and slowly neutralized using approximately 125 ml of 6M sodium hydroxide. If precipitation of an orange solid occurs, collect this as the product using vacuum filtration before extracting the solution with dichloromethane. The extracted solution was dried using magnesium sulfate and residual solvent was evaporated under vacuum pressure to give 0.7180g of product **(1)** in 31% yield. ^{1}H NMR (300 MHz, DMSO-D_6) δ 8.98

(dd, J = 4.7, 1.7 Hz, 2H), 8.39 (dd, J = 8.0, 1.9 Hz, 2H), 7.67 (dd, J = 8.0, 4.7 Hz, 2H). FTIR: 3061, 1685, 1560, 1418, 1414, 1293, 1205, 1116, 1011, 925, 807, 735, 668, 614, 540 (cm^{-1}).[16]

*2.2.2. Synthesis of 2,4-disulfoxide PIP **(2)***

A mixture of 1,10-phenanthroline-5,6-dione (0.315 g, 1.5 mmol, 1 equiv.), ammonium acetate (2.310 g, 30 mmol, 20 equiv.), and benzaldehyde-2,4-disulfonic acid disodium salt (0.465g, 1.5 mmol, 1 equiv.) was combined in a round bottom flask. Approximately 30 mL of glacial acetic acid was added to the round bottom flask and the mixture stirred under reflux for 24 hours. A solid yellow precipitate may form. Upon cooling, the solution was diluted with 60 ml of water and then neutralized with concentrated ammonia hydroxide to form a solid yellow precipitate around the pH of 6. The precipitate was collected from solution by vacuum filtration to give 0.4672 g of product **(2)** in 70% yield. ^{1}H NMR (300 MHz, DMSO-D_6) δ 9.05 (dd, J = 4.4, 1.7 Hz, 2H), 8.37 (dd, J = 8.1, 1.8 Hz, 2H), 7.88 (dd, J = 8.1, 4.5 Hz, 2H), 7.79 (dd, J = 8.0, 1.9 Hz, 1H), 7.40 – 6.85 (m, 4H). ^{13}C NMR (300 MHz, DMSO-D6) δ 172.0, 149.8, 148.4, 147.8, 143.6, 143.1, 130.5, 126.8, 126.5, 125.6, 123.7. FTIR (ATR): 3492, 3446, 3189, 3070, 1668, 1570, 1453, 1399, 1221, 1174, 1150, 1129, 1081, 1024, 806, 736, 691 (cm^{-1}).[2, 3, 5, 8, 24]

*2.2.3. Synthesis of 4-amino PIP **(3)***

The previously synthesized 4-nitro PIP ligand, 2-(4-Nitrophenyl)-1H-imidazo[4,5-f][1,10]phenanthroline (0.3806g, 1.115 mmol, 4.05 equiv.), was combined with 20ml of 200 proof ethanol in a 100 ml round bottom flask. The solution was sonicated so that all solids were dissolved before adding the palladium on carbon catalyst (0.0293g, 0.275 mmol, 1 equiv.) and a stir bar. The open vessel with the reaction mixture was then purged with argon gas before being sealed with a septum and further purged with a syringe punctured through center of the seal. A second and separate syringe was punctured through the septum cap for the dropwise addition of

hydrazine (0.7475 ml, 23.79 mmol, 87 equiv.). The solution was heated in an oil bath overnight while stirring at 70 °C. Upon cooling the solution was filtered to remove the pd/carbon, dissolved in chloroform, washed with water, and rotary evaporated to remove the ethanol and chloroform solvents. A dark red solid was obtained to give 0.271 grams of product **(3)** in 78 % yield. ^{1}H NMR (300 MHz, DMSO-D6) δ 9.16 – 8.88 (m, 6H), 8.85 – 8.63 (m, 1H), 8.51 (d, J = 21.6 Hz, 1H), 8.11 – 7.94 (m, 1H), 7.93 – 7.77 (m, 3H), 6.74 (d, J = 8.3 Hz, 1H). FT-IR (ATR): 3338, 3186, 2919, 2086, 1610, 1482, 1299, 1181, 1073, 958, 806, 740 (cm^{-1}).[6]

*2.2.4. Synthesis of 2-amino PIP **(4)***

The previously synthesized 2-nitro PIP ligand, 2-(2-Nitrophenyl)-1H-imidazo[4,5-f][1,10]phenanthroline (0.1850g, 0.54 mmol, 4.05 equiv.) was combined with 10ml of 200 proof ethanol in a 100 ml round bottom flask. The solution was sonicated so that all solids were dissolved before adding the palladium on carbon catalyst (0.0128g, 0.120 mmol, 1 equiv.) and a stir bar. The open vessel with the reaction mixture was then purged with argon gas before being sealed with a septum and further purged with a syringe punctured through center of the seal. A second and separate syringe was punctured through the septum cap for the dropwise addition of hydrazine (0.328 ml, 10.44 mmol, 87 equiv.). The solution was heated in an oil bath overnight while stirring at 70 °C. Upon cooling the solution was filtered to remove the pd/carbon. The filtered solution was dissolved in chloroform, washed with water, and rotary evaporated to remove the ethanol and chloroform solvents. A brown solid was obtained to give 0.1682g of product **(4)** in 48% yield. FT-IR (ATR): 3459, 3192, 2922, 2855, 2075, 1614, 1489, 1455, 1262, 1160, 1072, 1031, 756, 739 (cm^{-1}).[15]

*2.2.5. Synthesis of 4-hydroxy PIP **(5)***

A mixture of 1,10-phenanthroline-5,6-dione (0.2522g, 1.2 mmol, 1 equiv.), ammonium acetate (0.2076g, 25 mmol, 20.83 equiv.), and 4-hydroxybenzaldehyde (1.7 mmol, 1.42 equiv.) were combined in a round bottom flask according to the synthesis methods. Approximately 10 ml of glacial acetic acid was added to the round bottom flask and the mixture stirred under reflux for 3 hours. Upon cooling, after the reflux period, the solution was diluted with water. The acetic acid in solution was then neutralized using 10 ml of concentrated ammonia hydroxide to form a dark yellow precipitate. The solid precipitate was collected from solution by vacuum filtration to give 0.279g of product **(5)** in 53% yield. ^{1}H NMR (300 MHz, DMSO-D_6) δ 9.98 (s, 1H), 8.99 (dd, J = 4.3, 1.7 Hz, 2H), 8.86 (dd, J = 8.0, 1.7 Hz, 2H), 8.09 (d, J = 8.5 Hz, 2H), 7.78 (d, J = 5.0 Hz, 2H), 6.97 (d, J = 8.5 Hz, 2H). ^{13}C NMR (300 MHz, DMSO-D6) δ 159.5, 151.7, 148.1, 128.5, 121.7, 116.3. FT-IR (ATR): 3376, 3072, 1614, 1525, 1483, 1399, 1353, 1250, 1179, 1073, 1033, 960, 837, 801, 738, 692 (cm^{-1}).[22]

*2.2.6. Synthesis of 2-hydroxy PIP **(6)***

A mixture of 1,10-phenanthroline-5,6-dione **(1)** (0.315g, 1.5 mmol, 1 equiv.), ammonium acetate (2.310 g, 30 mmol, 20 equiv.), and the 2-hydroxybenzaldehyde (0.1832g, 1.5 mmol, 1 equiv.) were combined in a round bottom flask according to the synthesis methods. Approximately 30 ml of glacial acetic acid was added to the round bottom flask and the mixture stirred under reflux for 3 hours. Upon cooling, the solution was diluted with water. The acetic acid in solution was then neutralized using approximately 30 ml of concentrated ammonia hydroxide to form a pale-yellow solid. The solid precipitate was collected from solution by vacuum filtration to give 0.2554g of product **(6)** in 55% yield. ^{1}H NMR (300 MHz, DMSO-D_6) δ 9.04 (dd, J = 4.4, 1.6 Hz, 3H), 8.26 (dd, J = 8.2, 1.7 Hz, 1H), 7.86 (dd, J = 8.3, 4.4 Hz, 2H), 7.40

(td, J = 7.6, 1.6 Hz, 1H), 7.08 (d, J = 7.9 Hz, 3H). ^{13}C NMR (300 MHz, DMSO-D_6) δ 157.8, 151.2, 148.7, 143.6, 132.1, 126.8, 119.8, 117.8, 113.4. FT-IR (ATR): 3050, 1629, 1589, 1512, 1484, 1408, 1354, 1298, 1260, 1160, 1071, 959, 803, 737, 662 (cm^{-1}).[24]

CHAPTER 3: RESULTS AND DISCUSSION

3.1. CHARACTERIZATION OF PIP DERIVED LIGANDS

The experimental methods involved in this study seek to synthesize electron donating and water soluble PIP ligands to optimize $Eu(TTA)_3PIP$. Figure 7 shows the different derivations PIP ligands **(2-6)** that have been synthesized and characterized for further complexing with $Eu(TTA)_3$. The typical procedure for synthesizing a ligand was to reflux 1,10-phenanthroline-5,6-dione **(1)**, the appropriate aldehyde, and ammonium acetate in acetic acid. The reaction was then neutralized with aqueous NaOH until the pH was between 5-6, or the product precipitated from solution.

The appearance of ^1H NMR spectra varied greatly with the degree of protonation state of the ligand. Each ligand contains multiple heteroatoms that can be sites of protonation or hydrogen bonding. These resulted in spectral differences even for the same compound if they were collected at different pH's. Samples often contain water which also made the spectral analysis difficult. The absorption and emission data for each structural variation of the $Eu(TTA)_3PIP$ complex will be further used in future work to calculate the luminescent quantum yield (Φ). To complete the study, the quantum yield will be used to analyze how the coordinated ligand structure can optimize the luminescent emission of the $Eu(TTA)_3PIP$ complex.

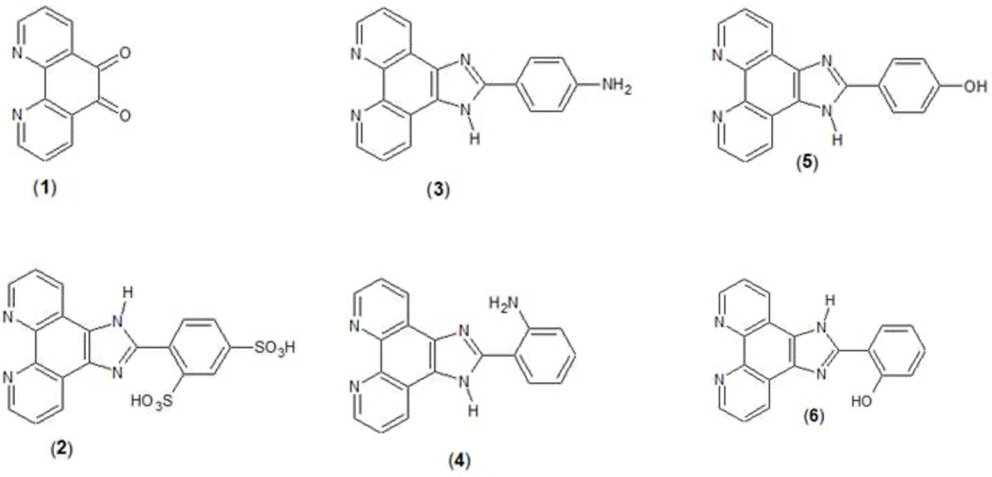

Figure 7. The starting material, phendione **(1)**, and PIP ligands **(2-6)** synthesized and characterized in the study.

*3.1.1. Structural Analysis of 1,10-phenanthroline-5,6-dione **(1)***

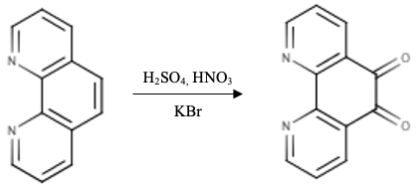

Figure 8. The reaction scheme for the synthesis of 1,10-phenanthroline-5,6-dione (1), the chelating structure and starting material in synthesizing the PIP ligand.

The structure of 1,10-phenanthroline-5,6-dione, was characterized by ^{1}H NMR and FT-IR spectra found in the supplemental material. The pure solid ranged in color from orange to red as a fine powder that should not be inhaled. The compound has a molecular weight of 210.192 g/mol and a molecular formula of $C_{12}H_6N_2O_2$. The ^{1}H NMR spectrum shows all six hydrogens located symmetrically in three different chemical environments. Three peaks for the

environments are observed in the aromatic region of the ^{1}H NMR spectrum, between 7 and 9.5 ppm. Each of the peaks were identified as a doublet of doublet with an integration of two hydrogens. The peak at 8.98 ppm, labeled as 1, represents the hydrogen environment alpha to the nitrogen in the 1,10-phenanthroline-5,6-dione ring system. Slightly up field at 8.39 ppm, peak 3, is from the hydrogen environment beta to the conjugated ketone. The peak furthest up field, peak 2, is from the hydrogen environment beta to the symmetrical nitrogen in the ring system. Residual water is also identified as a trace impurity in the ^{1}H NMR spectrum.

The FT-IR spectrum further identifies the specific functional groups present in the 1,10-phenanthroline-5,6-dione structure. Characterizing peaks are labeling in the FT-IR spectrum attached as supplemental material. The strong stretching frequency at 1685 cm^{-1} is from the symmetric aromatic ketones. While the vibrational modes at 1560, 1459 and 1414 cm^{-1} are the ring stretching vibrations from the C=C and C=N bonds. The strong band at 735 cm^{-1} is out of plane bending from the C-H bonds in the ring system. The structure of 1,10-phenanthroline-5,6-dione was confirmed from the acquired FT-IR and ^{1}H NMR spectra, further analysis using ^{13}C NMR spectroscopy was not performed.

3.1.2. Structural Analysis of 2,4-disulfoxide PIP ***(2)***

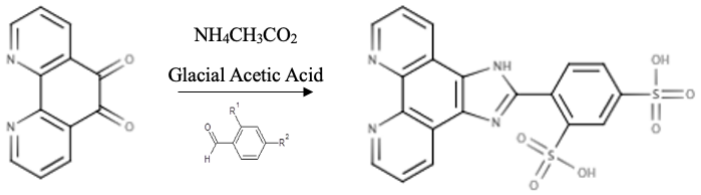

Figure 9. The reaction scheme for the synthesis of 4-(1H-imidazo[4,5-f]1,10-phenanthrolin-2-yl)benzene-1,3-disulfoxide (2).

The structure of the ligand, 2,4-disulfoxide PIP **(2),** was characterized by ^{1}H NMR, ^{13}C NMR, and FT-IR spectra found in the supplemental material. The compound has a molecular weight of 456.45 g/mol and a molecular formula of $C_{19}H_{12}N_4O_6S_2$. The solid resulted to be a fine powder which ranged in color from bright to pale yellow. The product was most readily soluble in water and dissolved in methanol upon agitation.

The signals observed in the ^{1}H NMR spectrum account for all detectable hydrogens in the 2,4-disulfoxide PIP structure. Three doublets of doublets are observed between 7.5 and 9.5 ppm that account for signals from the six hydrogens in the phenanthroline starting material. The remaining aromatic peaks between 6.9 and 7.4 ppm are signals from the three hydrogens in the 2,4-disulfoxide phenyl substitution. An observable integration of 4 phenyl hydrogens is due to hydrogen bonding that takes place between the secondary amino as well as an interfering detection of the hydrogen in the imidazole ring. A small peak is also seen at 12 ppm from the sulfonyl alcohol. Residual water as well as acetic acid are identified as trace impurities in the ^{1}H NMR spectrum. Ten peaks are observed in the ^{13}C NMR spectrum, accounting for the different carbon environments in the 2,4-disulfoxide PIP structure.

The FT-IR spectrum was used to identify the presence of sulfonate groups in the 2,4-disulfoxide PIP structure. The symmetric $S(=O)_2$ stretch is a broad band observed at 1175 cm^{-1} and followed by a second band at 1026 cm^{-1}. Detection of C-H aromatic vibrations was difficult due to residual water. Vibrations from the carbon sulfur bond are observed between 600 and 700 cm^{-1}. The structure of the 2,4-dsulfo PIP ligand was confirmed from the acquired FT-IR and NMR spectral data.

3.1.3. Structural Analysis of 4-amino PIP (3)

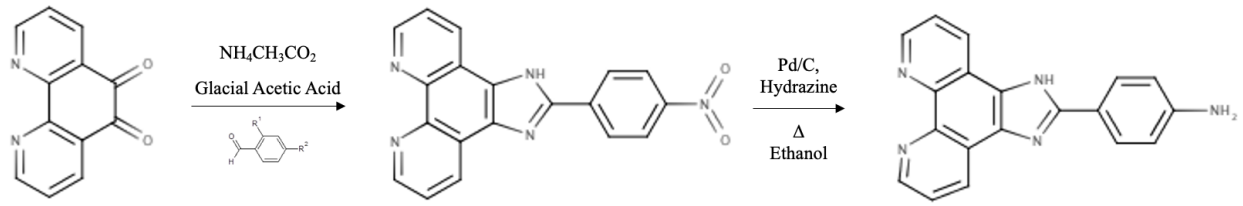

Figure 10. The reaction scheme for the synthesis of 4-(1H-imidazo[4,5-f]1,10-phenanthrolin-2-yl) p-aniline (3).

Ligand **(3)**, 4-amino PIP, was reduced from a previously synthesized ligand, 4-nitro PIP, and characterized using the FT-IR spectrum attached in the supplemental material. The compound has a molecular weight of 311.35 g/mol and a molecular formula of $C_{19}H_{13}N_5$. The solid resulted to be a fine powder which was deep red in color. The product was insoluble in D_2O and did not readily dissolve in DMSO. Solubility issues prevented further structural analysis using ^{13}C NMR spectroscopy.

The acquired FT-IR spectrum was used to identify the presence of the amino groups in the 4-amino PIP ligand structure. For the N-H bond in the primary amino substitution, all three modes of stretching, bending, and wagging are observed on the infrared spectrum. The N-H stretching is observed at 3338 and 3200 cm^{-1}, with a weaker signal that is blocked by the broad O-H band from residual water. The bending mode is observed at 1610 cm^{-1}, and the wagging mode at 740 cm^{-1}. The FT-IR spectrum of 4-nitro PIP, the ligand reduced to form 4-amino pip, was used comparatively for analysis. The vibrations at 1515 and 1336 cm^{-1} on the 4-nitro PIP spectrum are the N-O stretches. These vibrational modes are not present on the 4-amino PIP

spectrum, indicating the initial nitro groups were successfully reduced to form the 4-amino PIP ligand.

The signals observed in the attached ^{1}H NMR spectrum account for all detectable hydrogens in the 4-amino PIP structure. The compounds lack of solubility in D_2O and DMSO solvents did not allow for a well-defined ^{1}H NMR analysis. Hydrogen bonding from the primary amino substitution can also account for the unresolved spectrum. Three peaks are observed between 6.5 and 9.0 ppm that account for signals from the six hydrogens in the phenanthroline starting material. These peaks are shielded and shifted up field from the aromatic hydrogen signals closer to the 4-amino substitution. The broad peak from 9.14 – 8.90 ppm is from the hydrogen signals on the phenyl substitution. The integration of 5H can be attributed to the hydrogen bonding with the nitrogen in both the imidazole and the 4-amino group. Residual water as well as acetic acid are also identified as trace impurities in the ^{1}H NMR spectrum.

*3.1.4. Structural Analysis of 2-amino PIP **(4)***

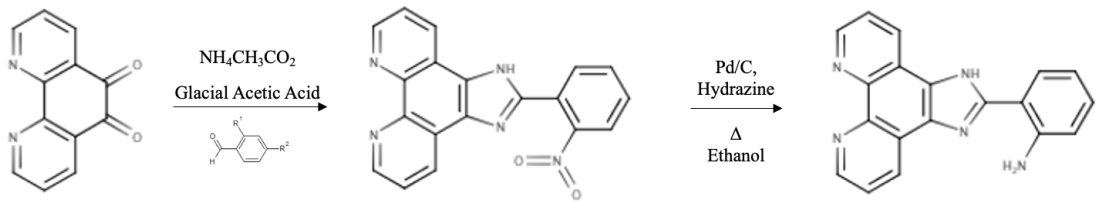

Figure 11. The reaction scheme for the synthesis of 4-(1H-imidazo[4,5-f]1,10-phenanthrolin-2-yl) o-aniline **(4)**.

Ligand **(4)** was reduced from 2-nitro PIP and characterized by the FT-IR spectrum found in the supplemental material. The compound has a molecular weight of 311.35 g/mol and a molecular formula of $C_{19}H_{13}N_5$. The solid resulted to be a fine powder that was wenge in color.

The product was insoluble in D_2O as well as DMSO. Solubility issues prevented further structural analysis using ^{1}H or ^{13}C NMR spectroscopy.

The FT-IR spectra was used to identify the presence of the amino groups in the 2-amino PIP ligand structure. For the primary amino substitution, the stretching, bending, and wagging vibrational modes of the N-H bond are observed. The N-H stretching mode is observed at 3459 and 3379 cm^{-1}, with a weaker signal that is blocked by the broad O-H band from residual water. The N-H bending mode is observed at 1614 cm^{-1} and the wagging mode at 739 cm^{-1}.

The FT-IR spectrum of 2-nitro PIP, the ligand reduced to form 2-amino pip, was used comparatively for analysis. The vibrations at 1530 and 1350 cm^{-1} on the 2-nitro PIP spectrum are the N-O stretches. These vibrational modes are not present on the 2-amino PIP spectrum, indicating the initial nitro groups were successfully reduced to form the 2-amino PIP ligand.

3.1.5. Structural Analysis of 4-hydroxy PIP ***(5)***

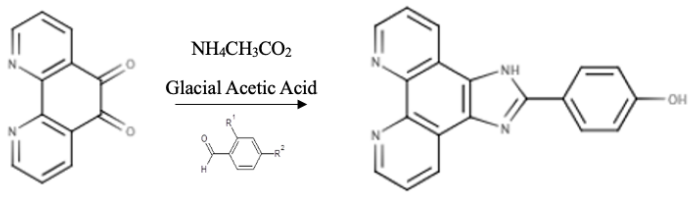

Figure 12. The reaction scheme for the synthesis of 4-(1H-imidazo[4,5-f]1,10-phenanthrolin-2-yl) p-phenol (5).

The structure of ligand **(5)**, 4-hydroxy PIP, was characterized using the ^{1}H NMR, ^{13}C NMR, and FT-IR spectra attached in the supplemental material. The compound has a molecular weight of 312.33 g/mol and a molecular formula of $C_{19}H_{12}N_4O$. The solid product resulted to be a fine powder that was ochre in color and soluble in DMSO, DCM, and partially in ethanol.

The signals observed in the ^{1}H NMR spectrum account for all detectable hydrogens in the ligand structure for 4-hydroxy PIP. A characterizing signal from the acidic phenol hydrogen is seen furthest down field near 10.0 ppm as a singlet. Two doublet of doublet peaks are observed around 9 ppm from two of the hydrogen environments in the phenanthroline structure of the ligand. The remaining proton signal from the phenanthroline structure is observed up field at 7.78 ppm in the form of a doublet. Signals from the aromatic phenol hydrogens are seen as doublet peaks at 8.09 and 6.67 ppm, both having an integration of 2 hydrogens. Residual solvents including water, acetic acid, and ethanol are identified in the ^{1}H NMR spectrum. Six peaks are identified and labeled in the ^{13}C NMR spectrum, accounting for the different carbon environments in the structure of the 4-hydroxy PIP ligand.

The FT-IR spectrum for 4-hydroxy PIP was acquired and used to identify the presence of the hydroxy group in the PIP ligand structure. The bonds involved in the substitution were characterized by the O–H stretch observed between 3500-3200 cm^{-1}, the in-plane O-H bending observed at 1483 and 1353 cm^{-1}, and the phenol C-O stretch at 1250 $cm^{-}1$. The dramatic drop in the baseline is from the aromatic C-H bonds and is observed in the peaks from 900-660 cm^{-1}.

3.1.6. Structural Analysis of 2-hydroxy PIP ***(6)***

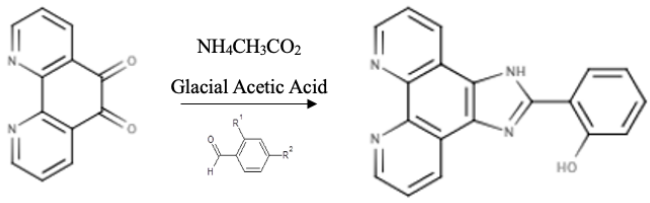

Figure 13. The reaction scheme for the synthesis of ligand (6), 4-(1H-imidazo[4,5-f]1,10-phenanthrolin-2-yl) o-phenol.

The structure of ligand **(6),** 2-hydroxy PIP, was characterized using the ^{1}H NMR, ^{13}C NMR, and FT-IR spectra attached in the supplemental material. The compound has a molecular weight of 312.33 g/mol and a molecular formula of $C_{19}H_{12}N_4O$. The solid product resulted to be a fine powder that was yellow in color and soluble in DMSO, dichloromethane and ethanol.

The signals observed in the ^{1}H NMR spectrum account for all detectable hydrogens in the ligand structure for **(6)**. Four peaks are observed furthest down field which account for the signals from the six hydrogens in the phenanthroline starting material. The remaining aromatic peak, up field at 7.08 ppm, is from three hydrogens in the 2-hydroxy phenyl group. The fourth hydrogen, closest to the 2-hydroxy substitution was difficult to detect on the spectrum due to potential hydrogen bonding with the lone pairs on the oxygen. In the ^{1}H NMR spectrum, residual water is identified as a trace impurity. Nine peaks are observed and labeled in the ^{13}C NMR spectrum, accounting for the different carbon environments in the structure of the 2-hydroxy PIP ligand.

The FT-IR spectrum for 2-hydroxy PIP was acquired and used to identify the presence of the hydroxy group in the PIP ligand structure. The bonds involved in the substitution were characterized by the phenol C-O stretch at 1260 $cm^{-}1$ and the in-plane O-H bending observed at 1408 and 1354 cm^{-1}. The characteristic O–H stretch between 3500-3200 cm^{-1} is not observed due to strong intermolecular interactions in the conjugated system. The dramatic drop in the baseline is from the aromatic C-H bond and is observed in the peaks from 900-660 cm^{-1}.

3.2. PROPERTIES OF COMPLEXED LIGANDS

3.2.1. Structural Variation of PIP Ligands

Each PIP ligand **(2-6)** was synthesized and structurally analyzed in part of an ongoing study of the luminescent properties associated with different phenyl substituents in a

Eu(TTA)$_3$PIP complex. For this part of the study, the functional groups were chosen specifically because of their electron donating and water-soluble properties. The sulfonate **(2)**, amino **(3,4)** and hydroxy **(5,6)** derived PIP ligands, with the specific water-soluble and electron donating substituents of interest, are highlighted pink in Figure 14**.**

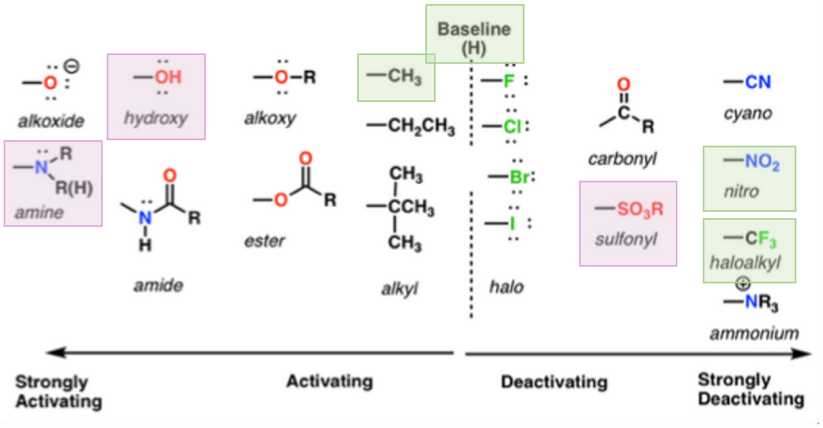

Figure 14. The range of structural variation in the phenyl substitution (-R) of the PIP ligand in the Eu(TTA)$_3$PIP complex. Water soluble (-SO3R) and electron donating (-OH, -NH2) substituents are highlighted pink.

Highlighted in green are electron withdrawing (-NO_2, -CF_3) and baseline (-H, -CH_3) functional groups from ligands that have been previously synthesized, complexed, and analyzed.[21] Among these ligands were the ortho and para positions for the haloalkyl, nitro, and methyl variations of the PIP ligand. The luminescent quantum yield was calculated for each of the previously studies ligands according to the methods described below.

3.3. CONCLUSIONS

The novel synthesis of the 2,4-disulfoxide PIP ligand **(2)** is of promising use for its noted property of water solubility. During the purification process, the collection of the pale-yellow

solid was difficult due to the noted water solubility of PIP ligand **(2).** The solid would begin to precipitate out of solution between a pH of 5 and 6. However, the ligand would dissolve back into solution if the pH were to approach the neutral range. This made the complete neutralization of all the acetic acid in the solution difficult and trace impurities are observed in the ^{1}H NMR spectra.

The appearance of NMR spectra varied depending on the protonation state of each PIP ligand when it was collected from solution. Each ligand contains multiple heteroatoms that can be sites of protonation or hydrogen bonding. These resulted in spectral differences even for the same compound if they were collected at a different pH. When collected, samples often contained residual water and acetic acid, which also made the spectral analysis difficult.

3.4. FUTURE WORK

3.4.1. Complexing PIP Derived Ligands

The PIP ligands (**2- 6)** should be used in preparation of the corresponding $Eu(TTA)_3PIP$ complexes. The quantitative absorption and emission data can then be collected for each complex and used to measure the luminescent quantum yield. These values should then be compiled with the quantum yield of the complexes from the previous work in this study.

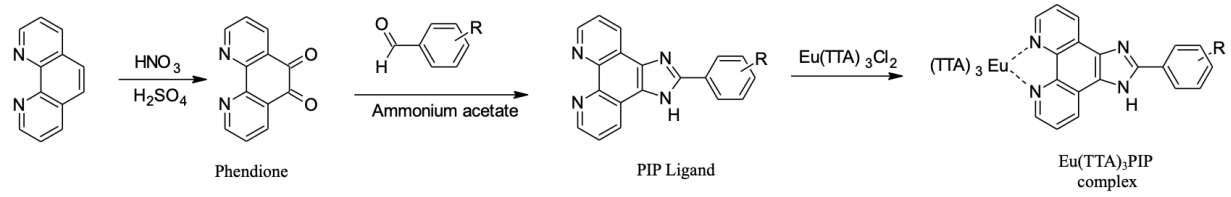

Figure 15. An overview of the synthesis methods in preparation of the $Eu(TTA)_3PIP$ complex.

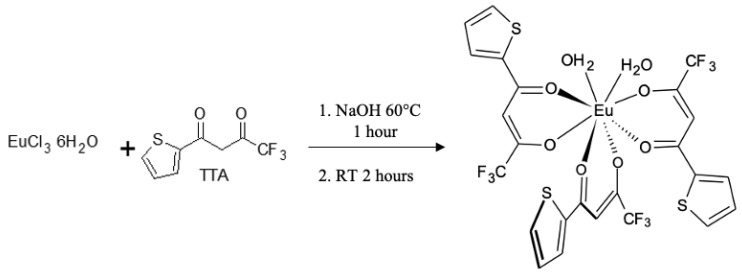

Figure 16. The reaction scheme for the synthesis of the Eu $(TTA)_3.2H_2O$ as starting material for the synthesis of the luminescent complex, $Eu(TTA)_3PIP$.

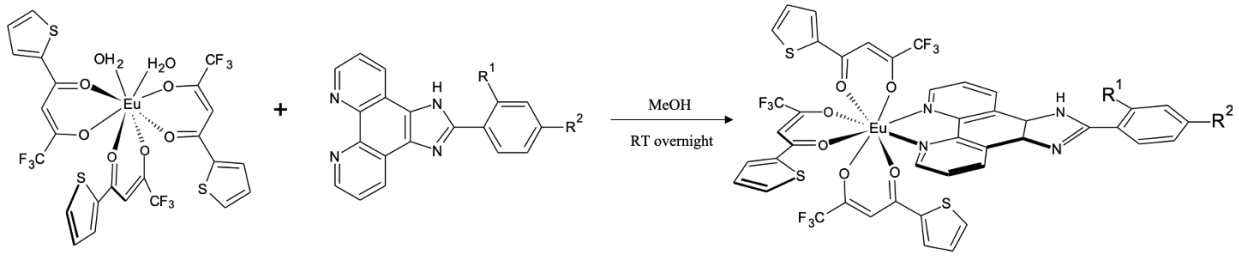

Figure 17. The reaction scheme for the synthesis of the luminescent lanthanide complex using the PIP ligand, $Eu(TTA)_3PIP$.

3.4.2. Luminescent Quantum Yield

Once the absorption and emission spectra are quantitatively collected for both the sample and a reference, the data can be used to calculate the luminescent quantum yield for each $Eu(TTA)_3PIP$ complex. The calculation for the luminescent quantum yield, $\boldsymbol{\phi}$, is listed below. The integrated intensity of emission ***(I)*** and the maximum light absorbance or optical density ***(OD)*** are obtained from the spectral data. These values are used to calculate the quantum yield in the equation below,

$$\boldsymbol{\phi = \phi_R \cdot \frac{I}{I_R} \cdot \frac{OD_R}{OD} \cdot \frac{n^2}{n^2{}_R}}$$

where the subscript **(R)** refers to any values corresponding to the reference sample. The value of **(ϕ_R)** is the known quantum yield for the reference and **(*n*)** is the refractive index of the solvent.

The reference, $Eu(TTA)_3 2H_2O$, is a well-studied complex with a consistent quantum yield value (**Φ** = 0.21). The reference as well as all previous $EuTTA_3PIP$ complexes have been previously dissolved in dichloromethane (**n** = 1.4244) for all quantum yield measurements. An excitation wavelength of 340 nm was measured as the maximum light absorbance and used in calculating the quantum yield of the samples. The excitation band of 340 nm corresponds to the absorption wavelength of TTA.[21] The emission range used for the integrated fluorescence intensity was from 500-750 nm. The absorption and emission data for the sample and the reference can be measured in triplicate on three separate days. The spectra can then be averaged to account for any possible environmental and instrumental error in the optical measurements.

3.4.3. Structural Analysis of Luminescent Properties

Table 1. The luminescent quantum yield (Φ) and energies of ΔE_{ET} and ΔE_{ISC} for previously synthesized derivations of the $Eu(TTA)_3PIP$ complex.[21]

Complex	ΔE_{ISC} (eV)	ΔE_{ET} (eV)	Φ%
$Eu(TTA)_3PIP$	0.8099	0.32717	46.14±3.0
$Eu(TTA)_3PIP$-2tolu	0.7527	0.32777	61.78±7.5
$Eu(TTA)_3PIP$-4tolu	0.7551	0.32757	60.80±7.3
$Eu(TTA)_3PIP$-2nitro	0.4661	0.32527	28.69±2.8
$Eu(TTA)_3PIP$-4nitro	0.2830	0.28097	34.64±6.3
$Eu(TTA)_3PIP$-2CF_3	0.7342	0.32627	60.03±8.5
$Eu(TTA)_3PIP$-4CF_3	0.6919	0.32757	55.06±4.7

To complete the study, all quantum yield values need to be measured and compiled with those of the previously analyzed $Eu(TTA)_3PIP$ complexes, see Table 1.[21] The values should be compared to determine the trends of luminescent efficiency for all structural variations of the

$Eu(TTA)_3$PIP complex. Computational methods should be used to calculate the associated energies of ΔE_{ET} and ΔE_{ISC} for each PIP derived complex. The energies of ΔE_{ET} and ΔE_{ISC} should be compared for each $Eu(TTA)_3$ PIP derived complex to analyze any trends and correspondence between the energies of ΔE_{ET}, ΔE_{ISC}, and the luminescent quantum yield of each complex.[10] If luminescence is optimized, water-soluble substituents are of interest for their use in biomedical labeling applications.

SUPPLEMENTAL INFORMATION

1,10-phenanthroline-5,6-dione **(1)**

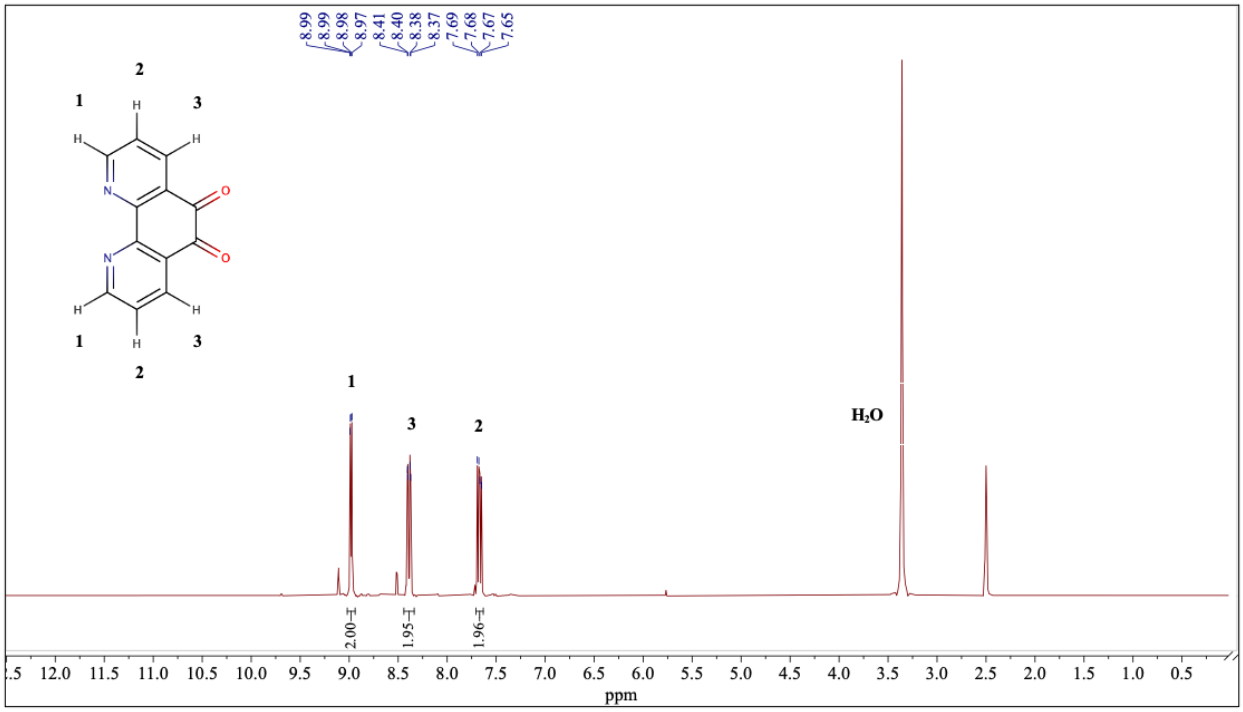

Figure 18. The ^{1}H NMR spectrum of **(1)** in DMSO-D_6.

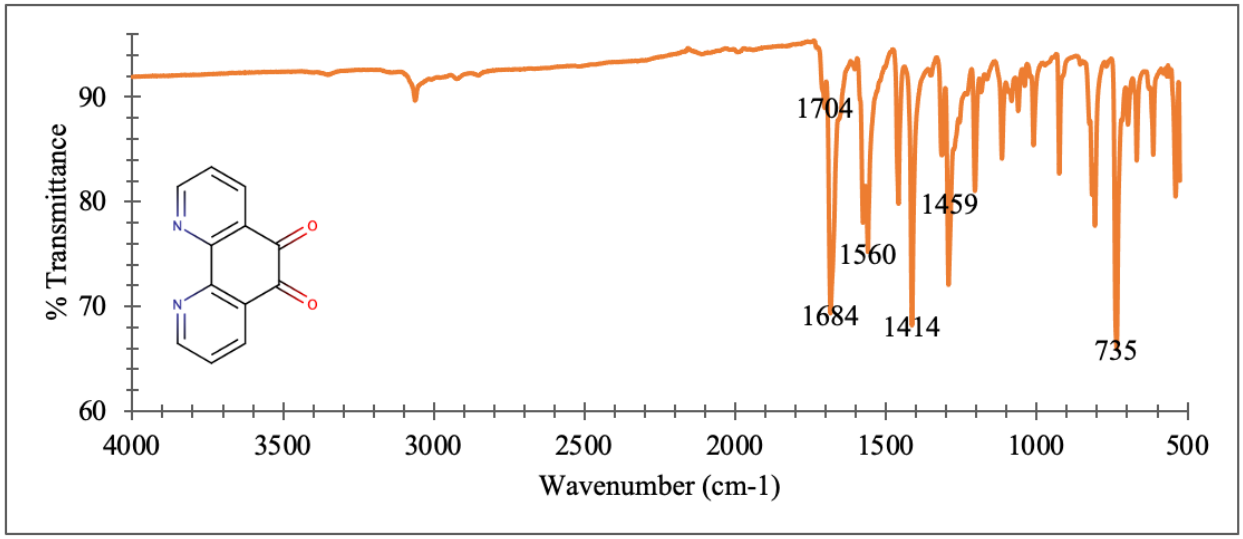

Figure 19. The FT-IR spectrum of **(1).**

4-(1H-imidazo[4,5-f]1,10-phenanthrolin-2-yl) benzene-1,3-disulfoxide **(2)**

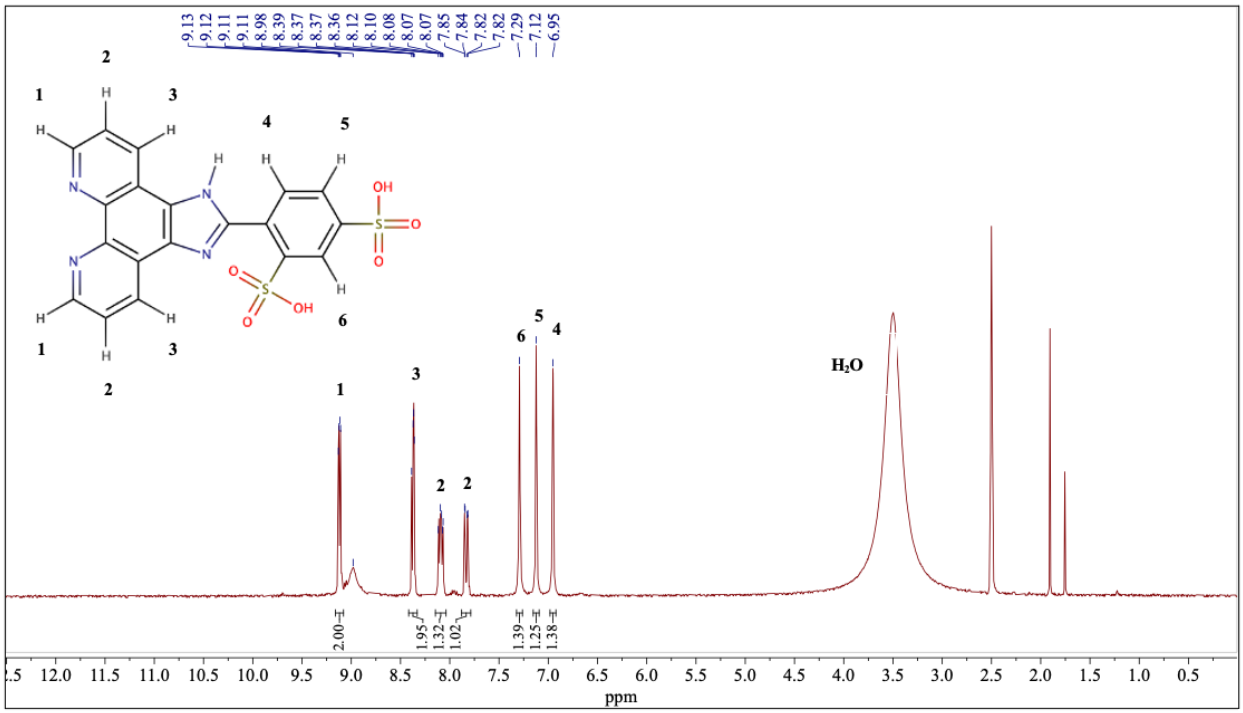

Figure 20. The ^{1}H NMR spectrum of **(2)** in DMSO-D_6.

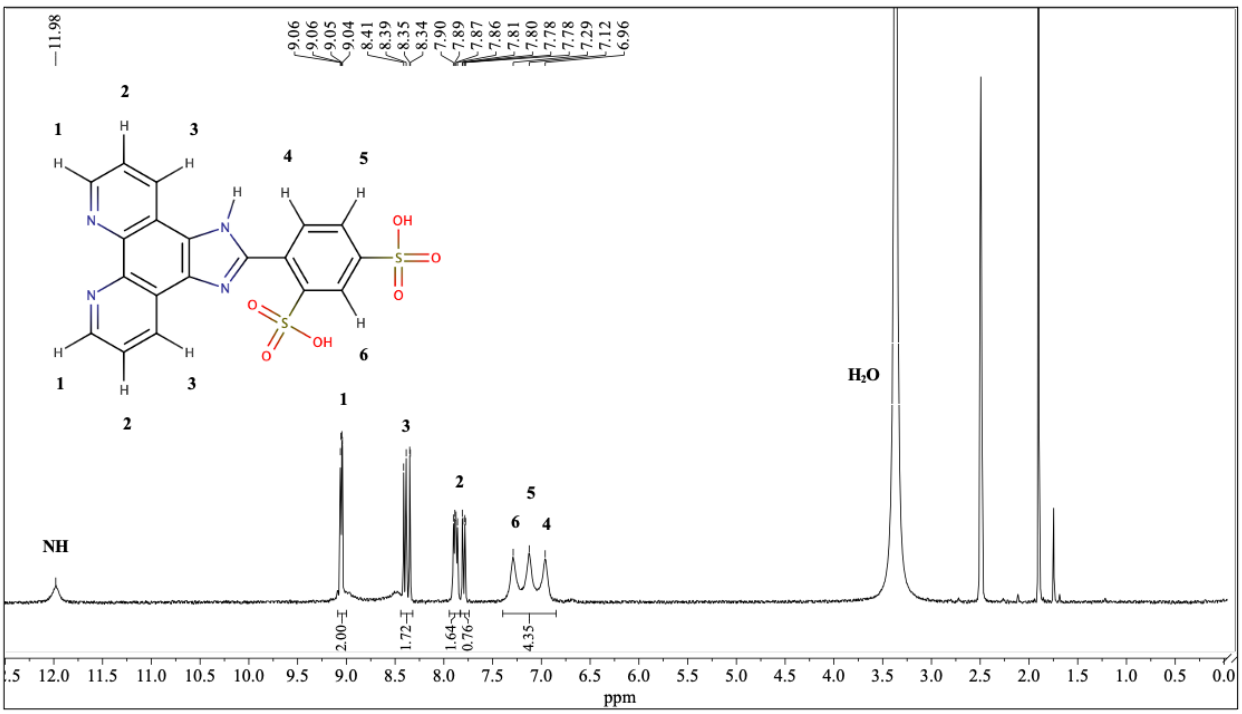

Figure 21. The 1H NMR spectrum of (2) in DMSO-D6.

4-(1H-imidazo[4,5-f]1,10-phenanthrolin-2-yl) benzene-1,3-disulfoxide **(2)**

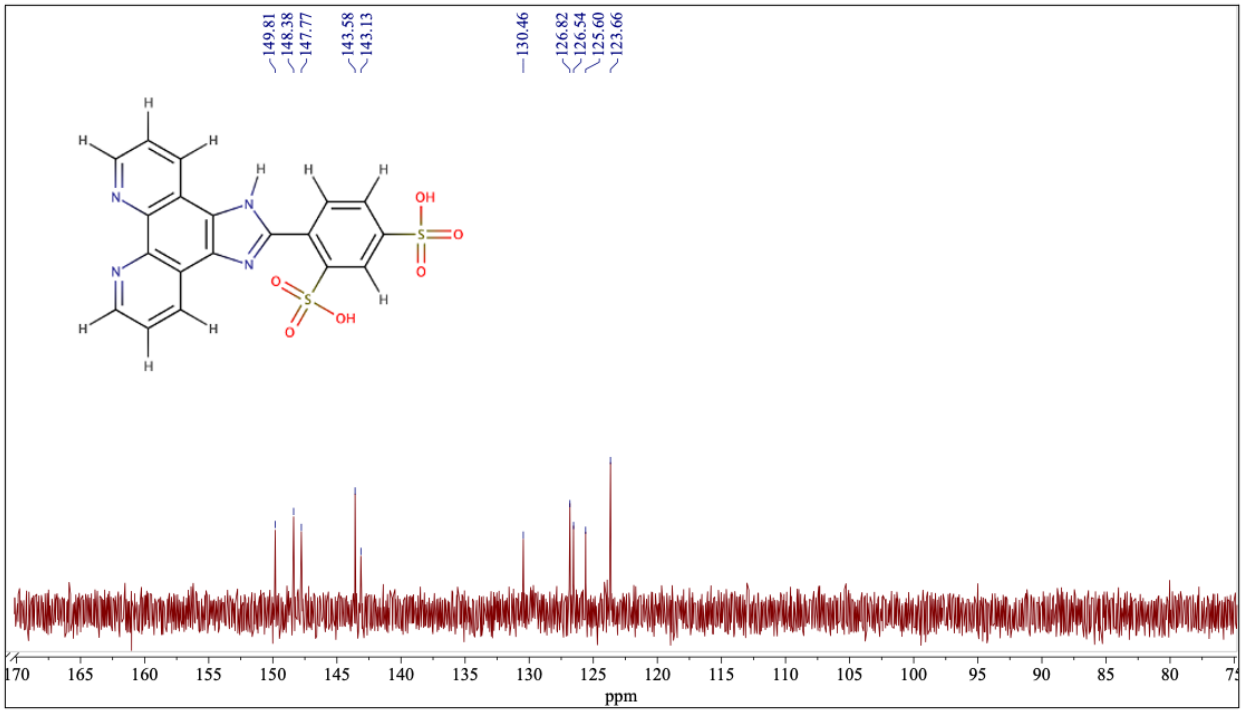

Figure 22. The ^{13}C NMR spectrum of **(2)** in DMSO-D_6.

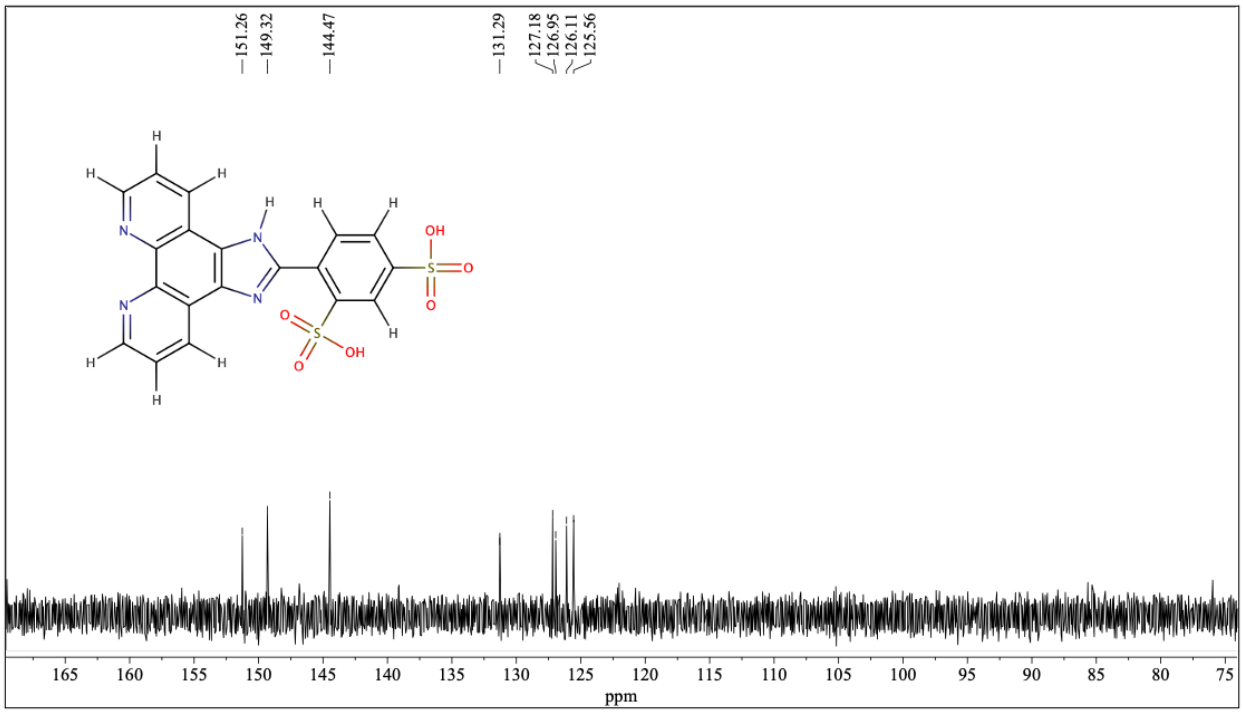

Figure 23. The ^{13}C NMR spectrum of **(2)** in DMSO-D_6.

4-(1H-imidazo[4,5-f]1,10-phenanthrolin-2-yl) benzene-1,3-disulfoxide **(2)**

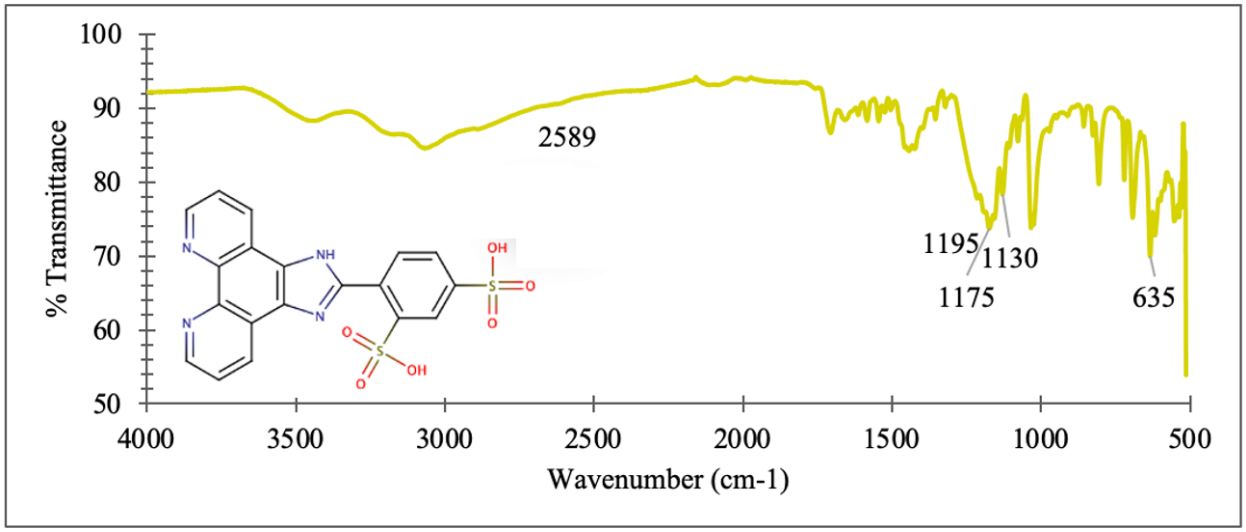

Figure 24. The FT-IR spectrum of **(2).**

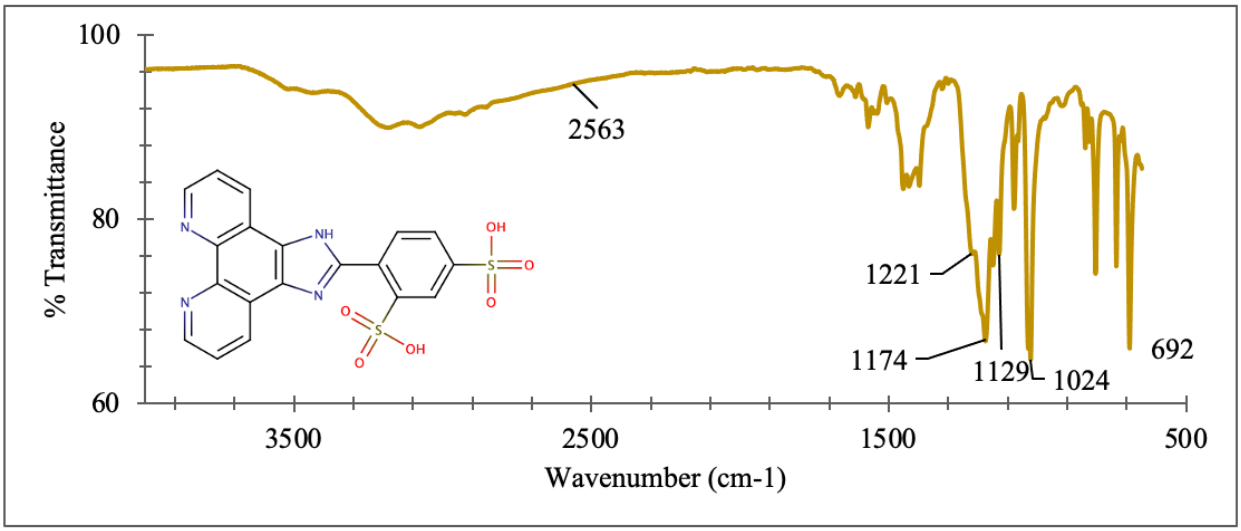

Figure 25. The FT-IR spectrum of **(2).**

4-(1H-imidazo[4,5-f]1,10-phenanthrolin-2-yl) p-aniline **(3)**

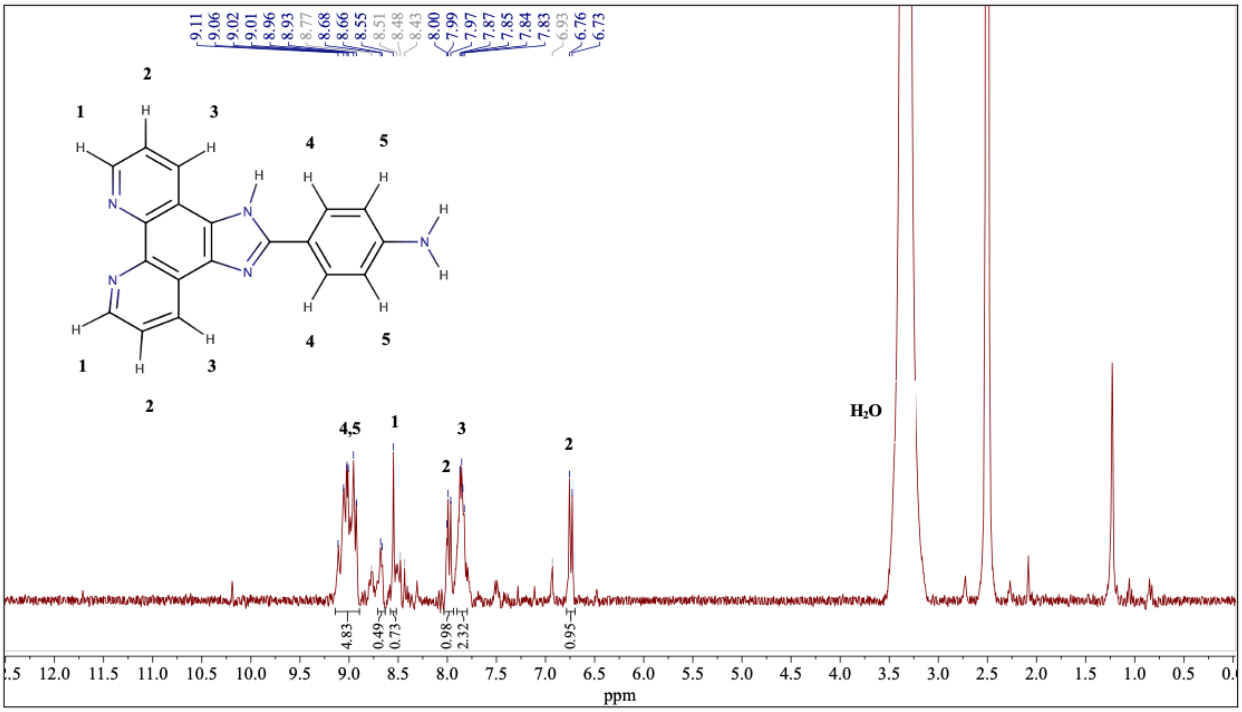

Figure 26. The ^{1}H NMR spectrum of **(3)** in DMSO-D_6.

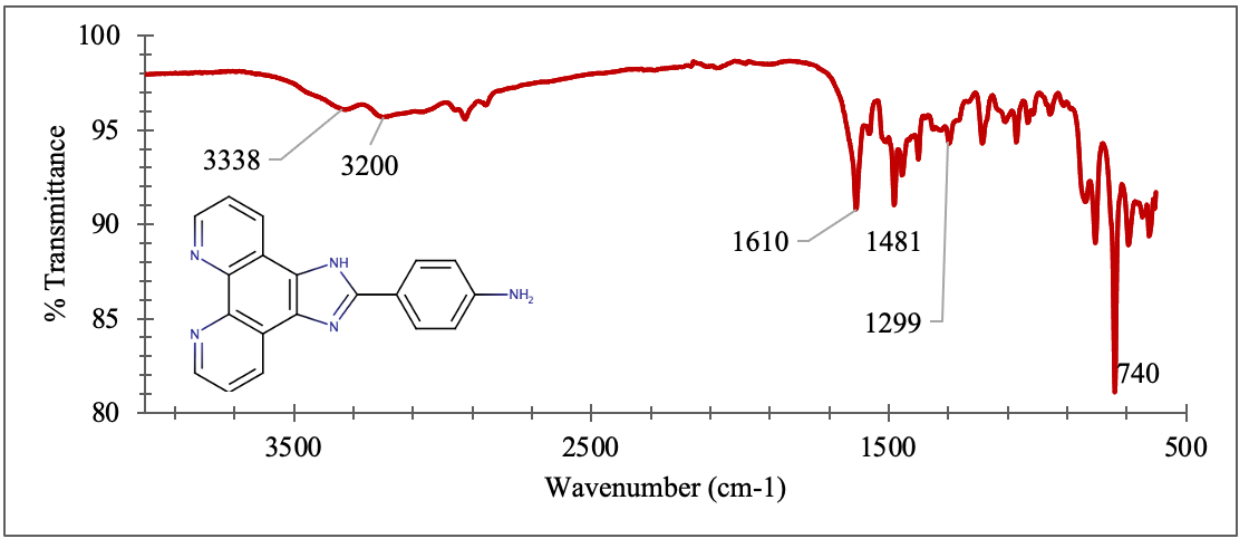

Figure 27. The FT-IR spectrum of **(3)**.

4-(1H-imidazo[4,5-f]1,10-phenanthrolin-2-yl) o-aniline (**4**)

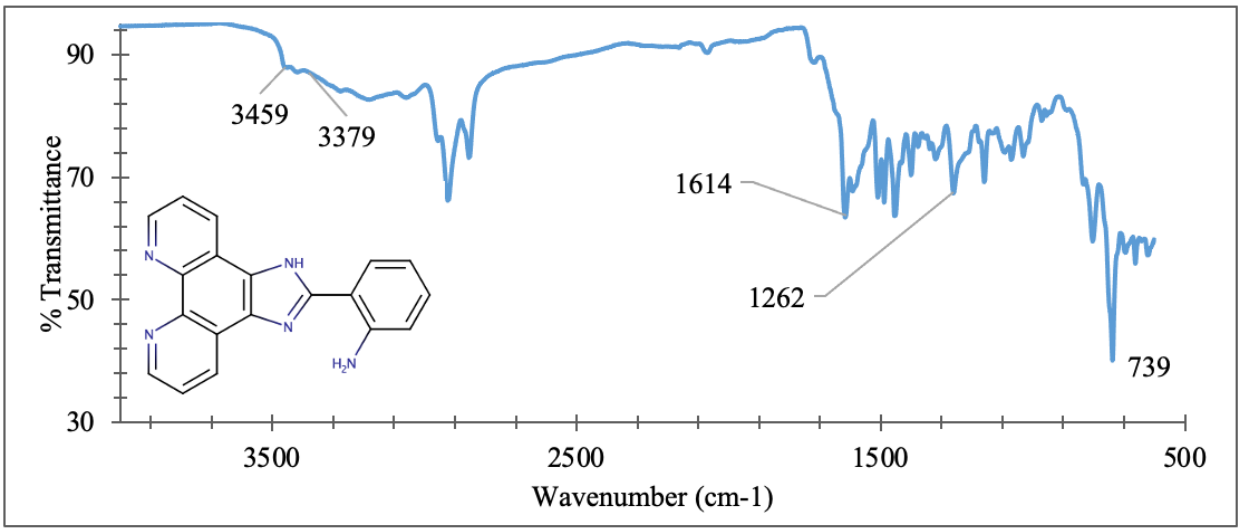

Figure 28. The FT-IR spectrum of **(4)**.

4-(1H-imidazo[4,5-f]1,10-phenanthrolin-2-yl) p-phenol **(5)**

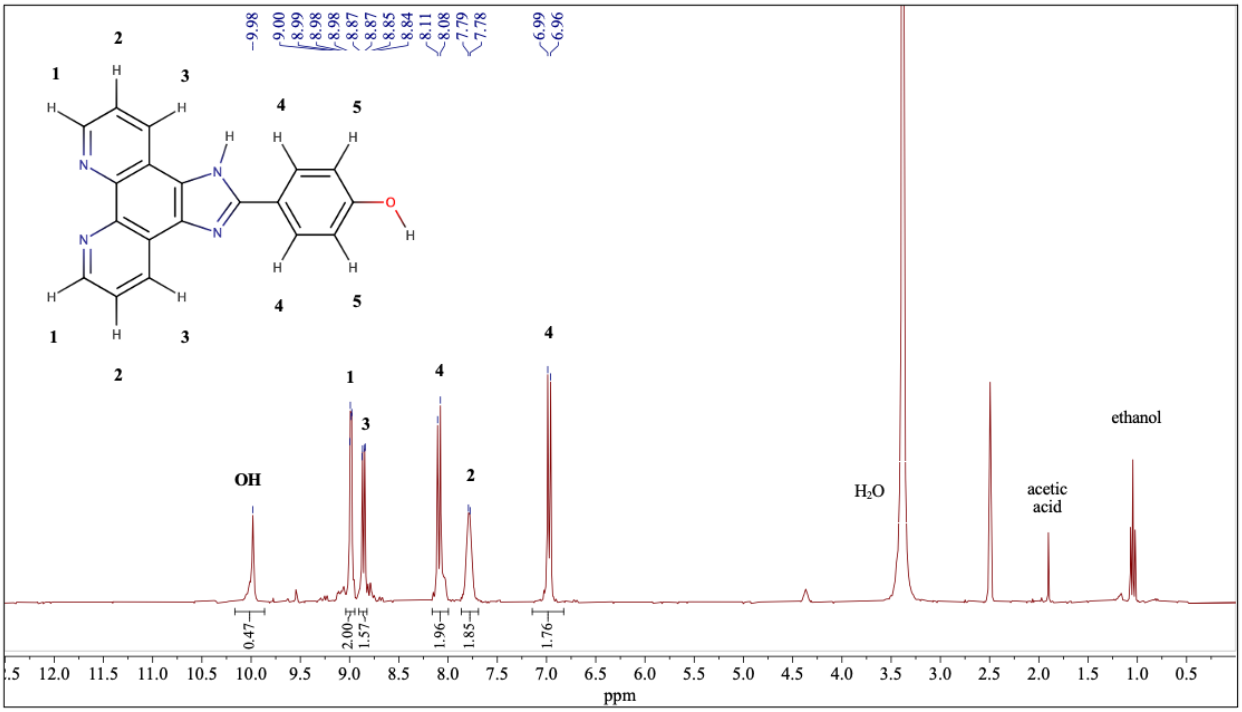

Figure 29. The 300 MHz ^{1}H NMR spectrum of **(5)** in DMSO-D_6.

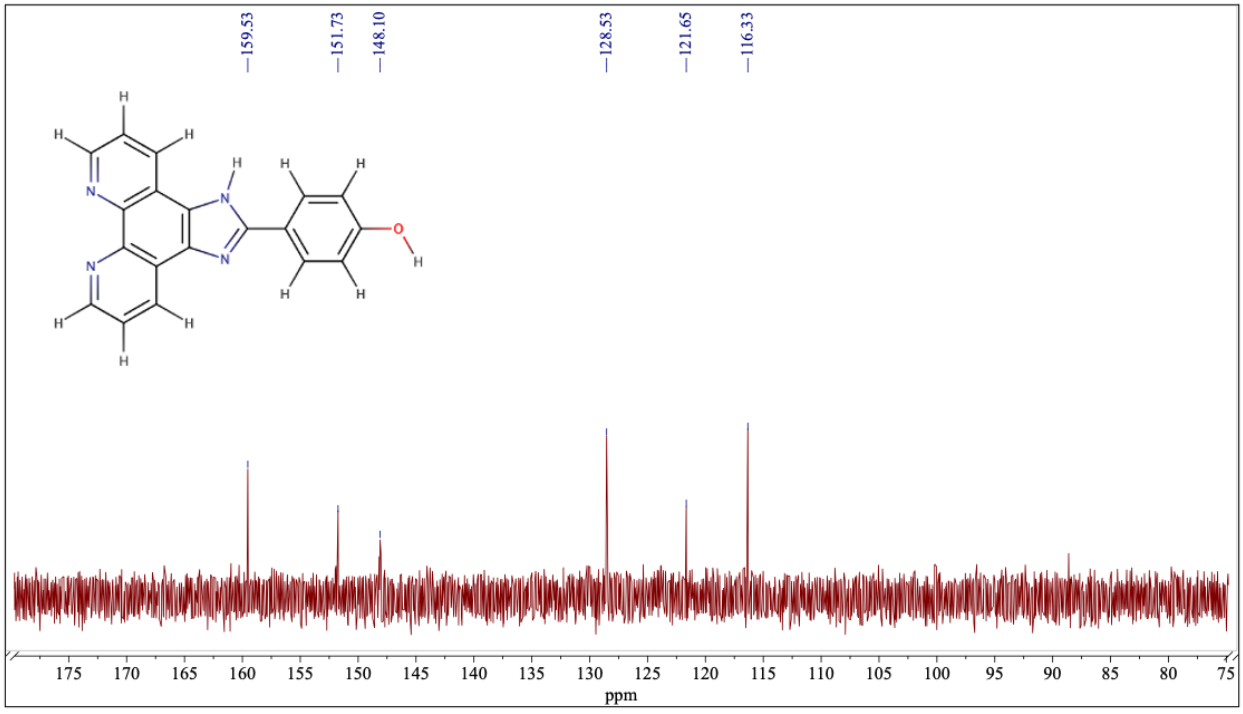

Figure 30. The 300 MHz ^{13}C NMR spectrum of **(5)** in DMSO-D_6.

4-(1H-imidazo[4,5-f]1,10-phenanthrolin-2-yl) p-phenol **(5)**

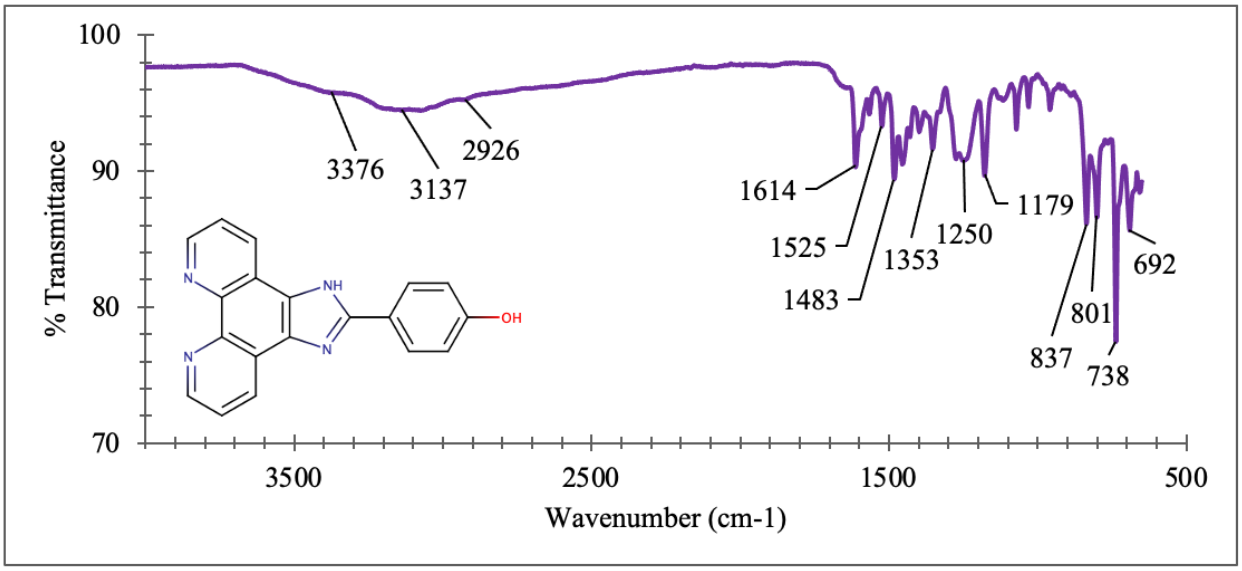

Figure 31. The FT-IR spectrum of **(5).**

4-(1H-imidazo[4,5-f]1,10-phenanthrolin-2-yl) o-phenol **(6)**

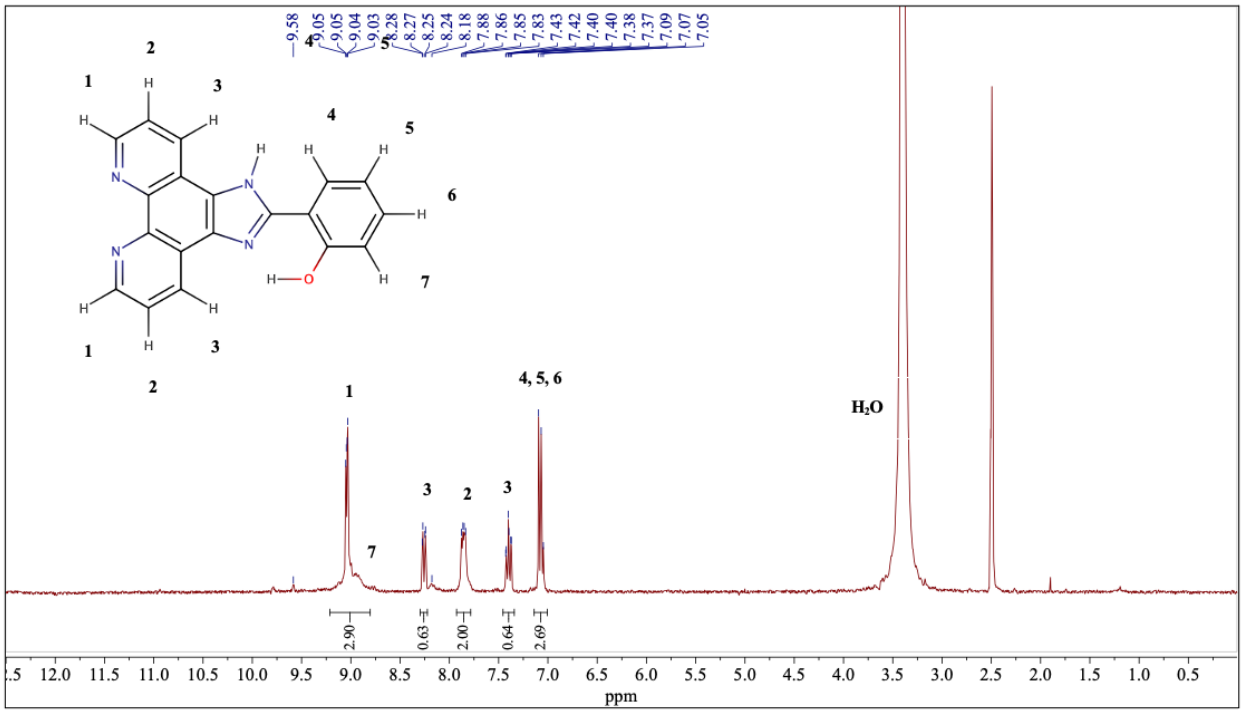

Figure 32. The ^{1}H NMR spectrum of **(6)** in DMSO-D_6.

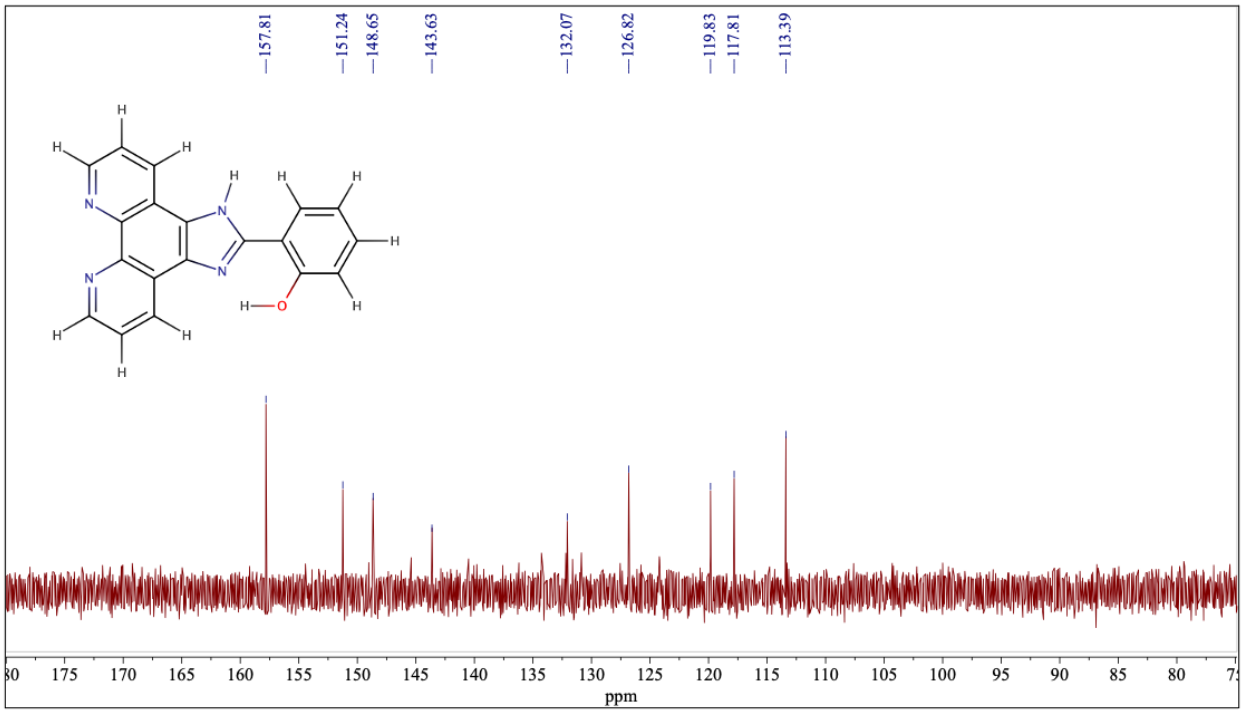

Figure 33. The 300 MHz ^{13}C NMR spectrum of **(6)** in DMSO-D_6.

4-(1H-imidazo[4,5-f]1,10-phenanthrolin-2-yl) o-phenol **(6)**

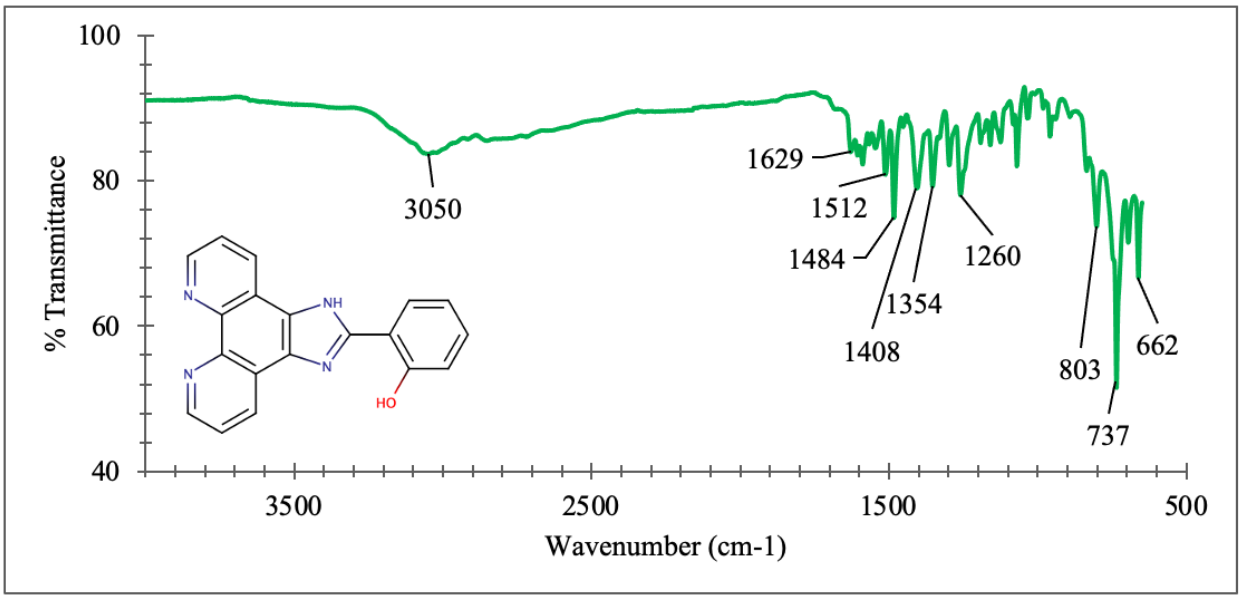

Figure 34. The FT-IR spectrum of **(6).**

REFERENCES

1. Aulsebrook, M. L. Lanthanide complexes for luminescence-based sensing of low molecular weight analytes. *Coordination Chemistry Reviews* **2018***, 375*, 191-220.
2. Bao, Q.; et al. Hydrothermal synthesis and crystal structure of four lead(II) coordination polymers with a carboxylate functionalized imidazophenanthroline derivative ligand. *Inorganica Chimica Acta.* **2013**, *405*, 51-57.
3. Bing, X.; et al. Hydrothermal Syntheses, Crystal Structures, and Luminescence Properties of Lanthanide-Based Coordination Polymers Constructed by Sulfonate Functionalized Imidazophenanthroline Derivative Ligand. *Cryst. Growth Des.* **2015***, 15*, 5, 2318–2329.
4. Binnemans, K.; et al. Hand Book on the Physics & Chemistry of Rare Earth Metals. **2005**, *35*, 107.
5. Cai, Z.; et al. Degenerate four-wave mixing determination of third-order optical nonlinearities of three mixed ligand nickel(II) complexes. *Journal of Molecular Structure.* **2011**, *1006*, 282-287.
6. Chakraborty, S.; et al. Mitochondria Targeted Protein-Ruthenium Photosensitizer for Efficient Photodynamic Applications. *Journal of the American Chemical Society.* **2017***, 139*, 6, 2512-2519.
7. Charbonniere, L. J. Luminescent Lanthanide Labels. *Current Inorganic Chemistry.* **2011**, *1*, 1, 2-16.
8. Chen, Q.; et al. Effect of pH on the construction of lead coordinated polymers. *Polyhedron.* **2014**, *81*, 517-524.
9. Døssing, A. Luminescence from Lanthanide(3+) Ions in Solution. *Eur. J. Inorg. Chem.* **2005**, *8,* 1425–1434.
10. De Silva, C.; et al. Correlation of Calculated Excited-State Energies and Experimental Quantum Yields of Luminescent Tb(III) β-Diketonates. *J. Phys. Chem. A.* **2008**, *112*, 20, 4527–4530.
11. De Silva, C.; et al. Adducts of lanthanide b-diketonates with 2,4,6-tri(2-pyridyl)-1,3,5-triazine: Synthesis, structural characterization, and photoluminescence studies. *Polyhedron.* **2007**, *26*, 1229.
12. Greco, C.; et al. Computational Investigation on the Spectroscopic Properties of Thiophene Based Europium β-Diketonate Complexes. *J. Chem. Theory Comput.* **2014***, 10*, 2, 767–777.

13. Handl, H. L.; et al. Lanthanide-based time-resolved Fluorescence of in cyto ligand–receptor interactions. *Analytical Biochemistry.* **2004**, *330*, 242–250.

14. Latva, M., T.; et al. Correlation between the Lowest Triplet State Energy Level of the Ligand and Lanthanide(III) Luminescence Quantum Yield. *J. Lumin.* **1997***, 75*(2), 149-169.

15. Liu, Y.-J.; et al. Cellular uptake, cytotoxicity, apoptosis, antioxidant activity and DNA binding of polypyridyl ruthenium(II) complexes. *Journal of Organometallic Chemistry.* **2011***, 696*(14), 2728-2735.

16. Paw, W.; Eisenberg, R. Synthesis, Characterization, and Spectroscopy of Dipyridocatecholate Complexes of Platinum. *Inorg. Chem.* **1997***, 36*, 11, 2287–2293.

17. Petoud, S.; et al. Brilliant Sm, Eu, Tb and Dy Chiral Lanthanide Complexes with Strong Circularly Polarized Luminescence. *J. Am. Chem. Soc.* **2007***, 129*, 77-83.

18. Quoc, M. L.; et al. Development of a fluorescent label tool based on lanthanide nanophosphors for viral biomedical application. *Adv. Nat. Sci: Nanosci. Nanotechnol.* **2012***, 3*.

19. Thompson, M. E.; et al. *Appl. Phys. Lett.* **1995***, 66*, 653.

20. Toseland, C. P. Fluorescent labeling and modification of proteins. *Journal of Chemical Biology.* **2013***, 6*, 3, 85-95.

21. Venturo, P. The Luminescent Properties of Europium Thenoyltrifluoroacetone Complexes with 2-Phenyl-1H-imidazo[4,5-f][1,10]phenanthroline Based Ligands. *Thesis.* **2020**.

22. Wei, C.-Y.; et al. 4-(1H-Imidazo[4,5-f]-1,10-phenanthrolin-2-yl)phenol-based G-quadruplex DNA binding agents: Telomerase inhibition, cytotoxicity and DNA-binding studies. *Bioorganic and Medicinal Chemistry.* **2013***, 21*, 11, 3379-3387.

23. Yuan, J.; Wang, G. Lanthanide Complex-Based Fluorescence Label for Time-Resolved Fluorescence Bioassay. *Journal of Fluorescence.* **2005***, 15*, 4, 559-568.

24. Zhang, W.-Z.; et al. 2-(1H-Imidazo[4,5-f][1,10]phenanthrolin-2-yl)phenol monohydrate. *Acta Cryst.* **2008***, 64*, o1331 .

25. Zhao, H.; et al. Syntheses, structures and luminescent properties of lanthanide coordination polymers assembled from imidazophenanthroline derivative and oxalate ligands. *Journal of Solid State Chemistry.* **2017**, 245, 67-73.